EFFECT OF MODE CONVERSION ON ULTRASONIC HEATING AT TISSUE INTERFACES

BY

BETH ANN HAKEN

B.S., University of Illinois, 1989

THESIS

Submitted in partial fulfillment of the requirements
for the degree of Master of Science in Electrical Engineering
in the Graduate College of the
University of Illinois at Urbana-Champaign, 1992

Urbana, Illinois

ABSTRACT

A number of investigators have observed localized heating by ultrasound near impedance discontinuities within tissues. It has been suggested that mode conversion to shear waves at impedance discontinuities and subsequent absorption of these waves in a very small distance were the explanations for this heating. A mathematical model for mode conversion at a plane interface between two viscoelastic media is presented. Longitudinal and shear properties are used to calculate the amount of mode conversion that occurs at muscle-bone and muscle-air interfaces. Shear waves in bone are found to be an important source of heating, but shear waves in the muscle provide a negligible effect on heating at the interface.

ACKNOWLEDGEMENTS

This work could not have been completed without the guidance of my advisor, Professor Leon Frizzell, the supportiveness of my parents, Janet and John Neundorfer, and the encouragement of my husband, Lippold Haken.

My appreciation is also extended to all of the people of the Bioacoustics Research Laboratory, especially Wanda Elliot, Bob Cicone, Billy McNeill, Ellen Chen, Felice Chu, Georgia Sebesta, Jing Hougen, Ilmar Hein, Linda Nostwick, Eric Chen, and Darshan Gandhi.

This work was supported in part by U. S. Public Health Service Grant No. GM 09933, a grant from the UIUC Hines VA Satellite Facility, and a National Science Foundation Graduate Fellowship.

TABLE OF CONTENTS

1. INTRODUCTION

As acoustic waves propagate through biological or other real media, they lose energy; the organized acoustic energy of the wave is transformed into heat. During ultrasonic imaging, heating is an unwanted side effect, but in physical therapy and in tumor hyperthermia, the production of heat is the desired result. Therefore an understanding of heating patterns produced by ultrasound fields can be useful in almost all applications, from forming safety standards for the power output of transducers in imaging systems to designing transducers for the production of specific heating profiles for therapy.

Many investigators have reported evidence for localized heating at tissue interfaces which have been irradiated by ultrasound[1-5]. Studies of ultrasound irradiation of livers have shown localized damage at the surface of the organ where the ultrasound beam exits that tissue[2-4]. Linke et al.[5] noted that changing the backing material of an irradiated organ from moistened gauze (which has acoustic properties similar to air because of the many small air spaces in it) to a water bath or a water bag (which have similar acoustic properties to soft biological tissues) eliminated the effect of excessive tissue destruction at the interface. Ultrasound transducers used for imaging and therapy produce longitudinal waves, but when these waves impinge obliquely on interfaces between media with different acoustic impedances, shear, or transverse, waves are transmitted

and reflected as well as longitudinal waves. The possible role of this mode conversion as a source of interfacial heating has been discussed[6-8].

Stiff materials such as bone are more capable of supporting shear waves than softer materials such as muscle because they have much larger shear stiffness. Therefore, an understanding of the effect of mode conversion is important for situations in which bone is irradiated. Pain associated with excess bone heating is a limiting factor in the hyperthermic treatment of some tumors[9]. Bone heating may be of particular concern for fetal exposures, since it is not possible to use ultrasonic imaging on fetuses without irradiating fetal bone tissue. Also, an understanding of absorbed power distribution within bone is fundamental to the determination of the mechanisms involved in accelerated healing of bone by ultrasound.

Chan et al.[10] indicated that shear waves generated in the bone when a longitudinal wave impinges on a muscle-bone interface must be considered in an analysis of heating by ultrasound. In his analysis, Chan considered shear waves in the soft tissues to be negligible. Filipczynski[11] has examined the role of shear waves at a tissue-air boundary and concluded that their contribution to heating is negligible in this special case. Frizzell and Carstensen[12] examined the more general case by allowing the possibility of shear waves in media on both sides of an interface. They studied mode conversion in the cases of longitudinal waves in

muscle incident on four different materials: air, water, cholesteryl linoleate, and bone.

Calculations in this study are based on measurements of the shear properties of soft body tissues at low megahertz frequencies[13]. The results of these measurements have since been confirmed and extended by Madsen and coworkers[14]. Utilizing these measurements, mode conversion and heating at muscle interfaces with air and bone have been computed for oblique incidence on a plane interface. The power deposition is calculated as a function of distance from the interface in each of these cases. Theoretical results confirm that shear waves contribute significantly to heating in hard tissues such as bone but shear waves in muscle provide a negligible contribution to heating at the interfaces examined.

2. THEORY

A longitudinal plane wave of infinite lateral extent is assumed to be obliquely incident on an infinite plane interface between two semi-infinite media. By choosing a coordinate system (Fig. 1) so that the propagation vectors for the waves lie in the x_1, x_2 plane, the analysis is greatly simplified by eliminating x_3 dependence in all expressions with no loss in generality. The two media are characterized by their complex longitudinal and shear propagation constants K_L, K_L' and K_S, K_S' and their densities ρ, ρ', respectively, where

$$K = \frac{\omega}{c} - j\alpha, \tag{1}$$

ω is the angular frequency, c is the real phase speed of the wave, and α its absorption coefficient. These constants can also be defined in terms of the complex bulk, B, and complex shear, μ, moduli of elasticity.

$$K_L = \sqrt{\frac{\rho\omega^2}{(B + \frac{4}{3}\mu)}} \tag{2a}$$

$$K_S = \sqrt{\frac{\rho\omega^2}{\mu}} \tag{2b}$$

These complex moduli may be expressed as

$$B = B_1 + j\omega B_2 \tag{3a}$$

$$\mu = \mu_1 + j\omega\mu_2 \tag{3b}$$

where B_1 and μ_1, real numbers, are the bulk and shear stiffness, respectively, and B_2 and μ_2, also real numbers, are the bulk and shear viscosity, respectively.

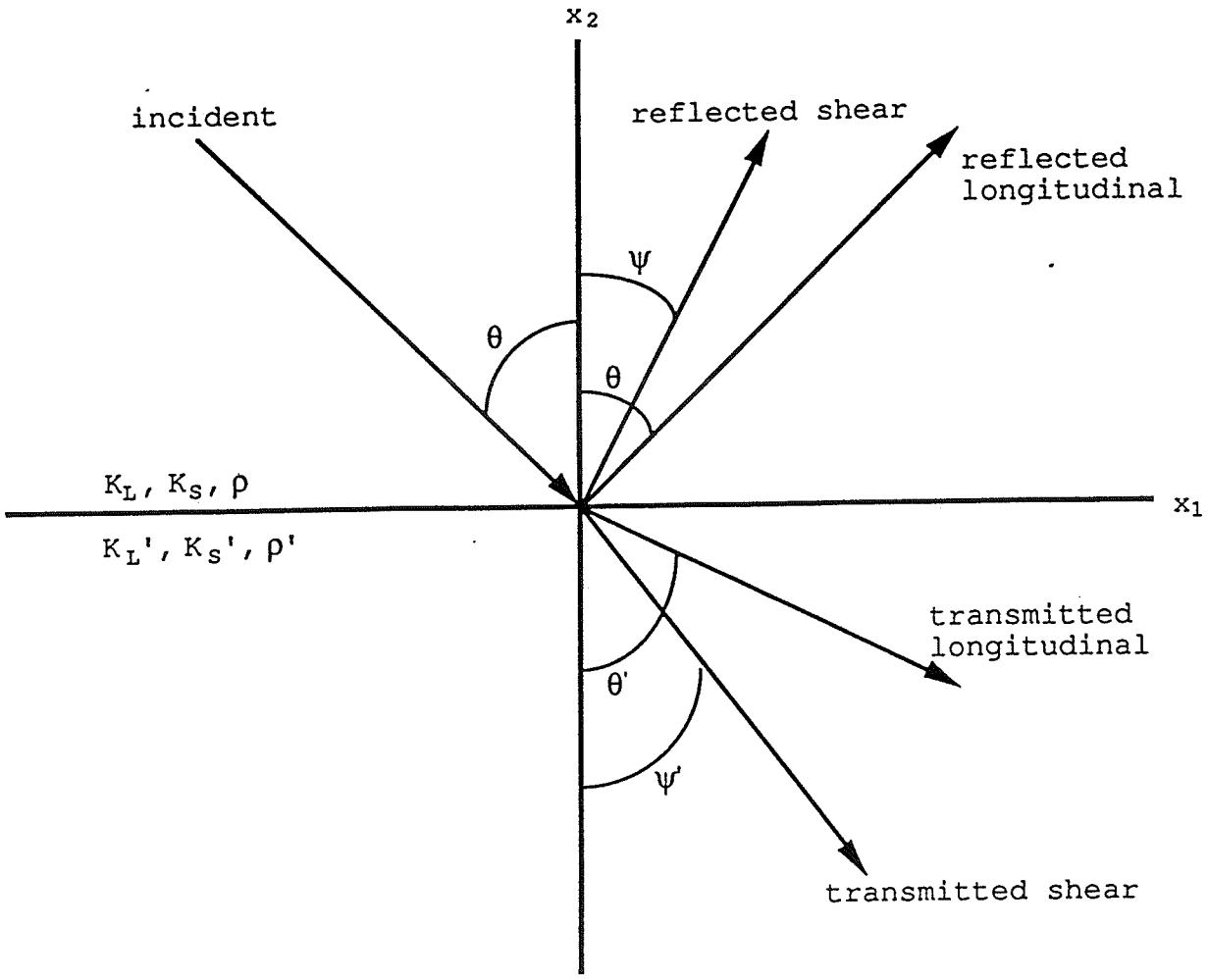

Figure 1. Reflected and transmitted longitudinal and shear waves for oblique incidence of a longitudinal wave on an interface between two semi-infinite media.

In general, a particle displacement vector ξ may be defined as the gradient of a scalar plus the curl of a vector,

$$\xi = \nabla\phi + \nabla \times \mathbf{A}, \tag{4}$$

where the scalar potential ϕ, which is associated with a longitudinal wave, and the vector potential $\mathbf{A}$, which is associated with a shear wave, are solutions of the wave equation for the medium. In the chosen coordinate system, only the component of $\mathbf{A}$

along the x_3 axis will be nonzero. It will be represented by the scalar a. Using the terminology of Cooper[15] for the potential coefficients, that is, the coefficients of the exponentials, the potentials are

the incident longitudinal,

$$\phi_I = \frac{L_I}{K_L} \exp[-jK_L(x_1\sin\theta - x_2\cos\theta)] \exp[j\omega t]$$
$$= \frac{1}{K_L} \Phi_I \exp[j\omega t], \tag{5a}$$

the reflected longitudinal,

$$\phi_R = \frac{L_I L_R}{K_L} \exp[-jK_L(x_1\sin\theta_R + x_2\cos\theta_R)] \exp[j\omega t]$$
$$= \frac{1}{K_L} \Phi_R \exp[j\omega t], \tag{5b}$$

the transmitted longitudinal,

$$\phi' = \frac{L_I L_T}{K_L'} \exp[-jK_L'(x_1\sin\theta' - x_2\cos\theta')] \exp[j\omega t]$$
$$= \frac{1}{K_L'} \Phi' \exp[j\omega t], \tag{5c}$$

the reflected shear,

$$a = \frac{L_I S_R}{K_S} \exp[-jK_S(x_1\sin\psi + x_2\cos\psi)] \exp[j\omega t]$$
$$= \frac{1}{K_S} A \exp[j\omega t], \tag{5d}$$

and the transmitted shear,

$$a' = \frac{L_I S_T}{K_S'} \exp[-jK_S(x_1\sin\psi' - x_2\cos\psi')] \exp[j\omega t]$$
$$= \frac{1}{K_S'} A' \exp[j\omega t], \tag{5e}$$

where the angles are defined in Fig. 1 and the potential coefficients L_R, L_T, S_R, and S_T are, in general, complex. From the potentials the components of the stress tensor (τ_{ij}) can be derived using Eq. (4) and the relationships between the potentials, the particle displacement, strain, and stress described in the following expressions.

$$\xi_1 = \frac{\partial \phi}{\partial x_1} + \frac{\partial a}{\partial x_2} \tag{6a}$$

$$\xi_2 = \frac{\partial \phi}{\partial x_2} - \frac{\partial a}{\partial x_1} \tag{6b}$$

$$\xi_3 = 0 \tag{6c}$$

$$s_{ij} = \frac{1}{2}\left(\frac{\partial \xi_i}{\partial x_j} + \frac{\partial \xi_j}{\partial x_i}\right) \tag{7}$$

$$\tau_{ij} = \lambda \delta_{ij}(s_{11} + s_{22} + s_{33}) + 2\mu s_{ij} \tag{8a}$$

$$\lambda = B - \frac{2}{3}\mu \tag{8b}$$

where s_{ij} are the components of the strain tensor, τ_{ij} are the components of the stress tensor, and δ_{ij} is zero for $i \neq j$ and one for $i = j$.

Boundary conditions are applied to determine the angles and potential coefficients. So that there is no separation at the interface, the normal (x_2) component of the particle displacement must be continuous across the boundary. The tangential (x_1) component of the particle displacement must be continuous across the boundary so that there is no slippage. Finally, using the divergence theorem, boundary conditions on the stress are determined which require that force is continuous across the boundary so that the interface does not undergo infinite acceleration[12]. These boundary conditions are expressed by the following four equations for the geometry described here.

$$\xi_2 = \xi_2' \tag{9a}$$

$$\xi_1 = \xi_1' \tag{9b}$$

$$\tau_{21} = \tau_{22}' \tag{9c}$$

$$\tau_{22} = \tau_{22}' \tag{9d}$$

Application of the boundary conditions yields the Snell's law relations that can be used to determine the complex angles of reflection and refraction,

$$K_L \sin\theta_R = K_L \sin\theta \tag{10a}$$

$$K_S \sin\psi = K_L \sin\theta \tag{10b}$$

$$K_L' \sin\theta' = K_L \sin\theta \tag{10c}$$

$$K_S' \sin\psi' = K_L \sin\theta \tag{10d}$$

(note that $\theta_R = \theta$). Using Eq. (10), the boundary conditions simplify to the following relations which determine the coefficients of the potentials L_R, L_T, S_R, and S_T.

$$\begin{bmatrix} \sin\theta & \cos\psi & -\sin\theta' & \cos\psi' \\ \cos\theta & -\sin\psi & \cos\theta' & \sin\psi' \\ -\frac{\rho\omega}{K_L}\cos 2\psi & \frac{\rho\omega}{K_S}\sin 2\psi & \frac{\rho'\omega}{K_L'}\cos 2\psi' & \frac{\rho'\omega}{K_S'}\sin 2\psi' \\ \frac{\rho\omega K_L}{K_S^2}\sin 2\theta & \frac{\rho\omega}{K_S}\cos 2\psi & \frac{\rho'\omega K_L}{K_S'^2}\sin 2\theta' & \frac{\rho'\omega}{K_S'}\cos 2\psi' \end{bmatrix} \begin{bmatrix} L_R \\ S_R \\ L_T \\ S_T \end{bmatrix}$$

$$= \begin{bmatrix} -\sin\theta \\ \cos\theta \\ \frac{\rho\omega}{K_S}\cos 2\psi \\ \frac{\rho\omega K_L}{K_S^2}\sin 2\theta \end{bmatrix} \tag{11}$$

Here, the coefficient L_I has been chosen such that the magnitude of the incident intensity is unity. As noted by Chan et al.[10], the total ultrasonic intensity is

$$\mathbf{I} = \frac{1}{2} \mathrm{Re}[\mathbf{u} \cdot \mathbf{T}^*] \tag{12}$$

where

$$\mathbf{u} = \frac{\partial \xi}{\partial t} \tag{13}$$

is the particle velocity, $\mathbf{T}$ is the second-order stress tensor whose components are defined in Eq. (8a), and * denotes the complex conjugate. The rather lengthy expressions for the intensities in terms of the potential coefficients are provided in Appendix A. Finally, the power loss, or power deposition, per unit volume is

$$P_L = -\nabla \cdot \mathbf{I}. \tag{14}$$

Equations (12) and (14) contain terms that can be associated with purely longitudinal waves (terms involving products of scalar potentials) and purely shear waves (terms involving products of vector potentials), but, in addition, several "cross terms" involve products of the vector and scalar potentials, or products of the incident and reflected scalar potentials (see Appendix A). In lossless media the cross terms cancel each other, and the two types of waves are resolved into shear and longitudinal contributions to the intensity and to the power deposition. However, in the general case in which both media are lossy (have nonzero absorption coefficients), the cross terms do not cancel and must be included to maintain energy conservation at the interface and to obtain the correct form for the power deposition.

Equation (14) gives the power deposition per unit volume in the general case. It would be interesting to know what fractions

of this power deposition and resultant heating should be attributed to longitudinal and to shear waves. In the past, two similar approaches have been taken to answer this question. In each, the intensities were divided into longitudinal and shear components and separately inserted into Eq. (14). Since the intensities contain cross terms, the assignment of the energy associated with these terms presented a problem. Chan et al.[10] assigned the energy in these cross terms in proportion to the amplitudes of the vector and scalar potentials and used the results to calculate power deposition. Frizzell and Carstensen[12] assigned the cross terms to the longitudinal and shear intensities in proportion to the squares of the amplitudes, or, in other words, in proportion to the purely longitudinal and the purely shear terms of the intensity. As will be seen, these arbitrary simplifications of the problem result in loss of information about the power deposition and demonstrate, in part, that the heating rate involves interactions of shear and longitudinal particle velocities and stresses.

3. COMPARISONS TO OTHER WORK

Several tests of the theory were performed. First, it was determined that the sum of the normal components of the transmitted and reflected intensities equaled the normal component of the incident intensity. Thus, conservation of energy at the boundary is satisfied. Second, for the lossless case, numerical results for the normal components of intensities, that is, the transmitted and reflected power coefficients, obtained using this theory agreed with those of Ewing et al.[16].

Nyborg[18] developed relations for the power deposition in two different media, one exhibiting no shear viscosity and one with no bulk viscosity. In each case two longitudinal plane waves propagated at right angles to each other. This is equivalent to the situation in this study for the incident medium when the angle of incidence is 45°, $L_R = 1$, $S_R = L_T = S_T = 0$, and $\mu_2 = 0$ or $B_2 = 0$, respectively. Unlike Nyborg's analysis, in this case the wave amplitude decays with distance. However, a meaningful comparison was possible by considering small values of the absorption coefficient and small distances from the interface. Also, Nyborg assumed unit pressure amplitude instead of unit intensity magnitude. A direct comparison was still possible by using the values of density and longitudinal speed (because only longitudinal waves are propagating) to determine the corresponding intensity from

$$|I| = \frac{|P|^2}{2\rho c_L} \quad . \tag{15}$$

The plots in Fig. 2 show that numerical results from each theory are indistinguishable. The numerical values of the media parameters used in these calculations may be found in Table 1.

Table 1. Numerical values used in the comparison to Nyborg[18]. Frequency is 2 MHz. Incident intensity is 1 W/cm^2.

	zero shear viscosity (Fig. 2a)	zero bulk viscosity (Fig. 2b)
B (g/s^2)	$2.608681\times10^{10} + j8.993428\times10^{7}$	$2.608681\times10^{10} + j0$
μ (g/s^2)	$3.989381\times10^{5} + j0$	$3.989381\times10^{5} + j2.9877995\times10^{6}$
K_L (cm^{-1})	$81.59986 - j0.1406545$	$81.60022 - j6.230474\times10^{-3}$
K_S (cm^{-1})	$2.086669\times10^{4} + j0$	$5.711987\times10^{3} - j5.000000\times10^{3}$

With bulk viscosity only, Nyborg calculated power deposition with maximum value "$\frac{4\alpha}{\rho_o c}$" and zeros at "$\frac{\pi c\sqrt{2}}{\omega}\left(n + \frac{1}{2}\right)$", (n = 0, 1, 2, ...), corresponding to

$$P_{L,max} = -8\ \mathrm{Im}\{K_L\} \tag{16a}$$

for unit incident intensity and

$$x_2 = \frac{\pi\sqrt{2}}{\mathrm{Re}\{K_L\}}\left(n + \frac{1}{2}\right), \tag{16b}$$

respectively. With shear viscosity only, Nyborg calculated power deposition with maximum value "$\frac{3\alpha}{\rho_o c}$" at "$\frac{\pi c\sqrt{2}}{\omega}\left(n + \frac{1}{2}\right)$" which corresponds to

$$P_{L,max} = -6\ \mathrm{Im}\{K_L\} \tag{16c}$$

and

$$x_2 = \frac{\pi\sqrt{2}}{\mathrm{Re}\{K_L\}}\left(n + \frac{1}{2}\right) \tag{16d}$$

in this work and minimum value "$\frac{\alpha}{\rho_o c}$" at "$\frac{\pi c\sqrt{2}}{\omega}$ n" which corresponds to

$$P_{L,min} = -2\ \mathrm{Im}\{K_L\} \tag{16e}$$

and

$$x_2 = \frac{\pi\sqrt{2}}{\mathrm{Re}\{K_L\}} \tag{16f}$$

here.

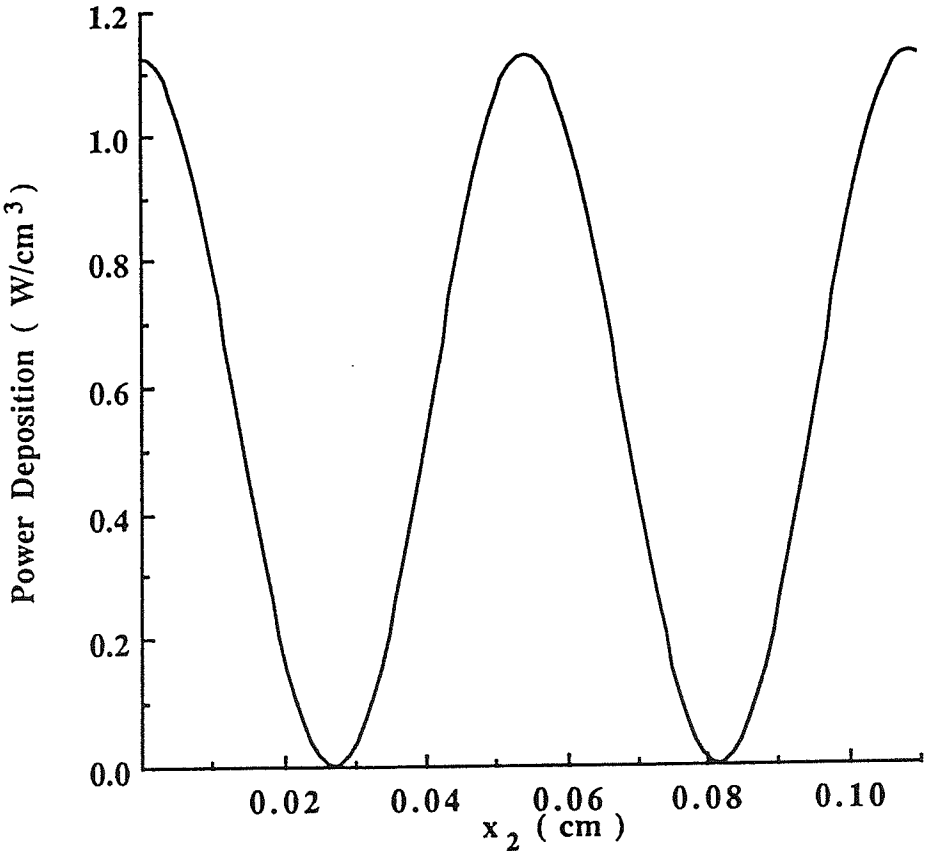

Figure 2a. Power deposition versus distance from the interface in the incident medium for zero shear viscosity using Eq. (14); same as Nyborg's[18] plot.

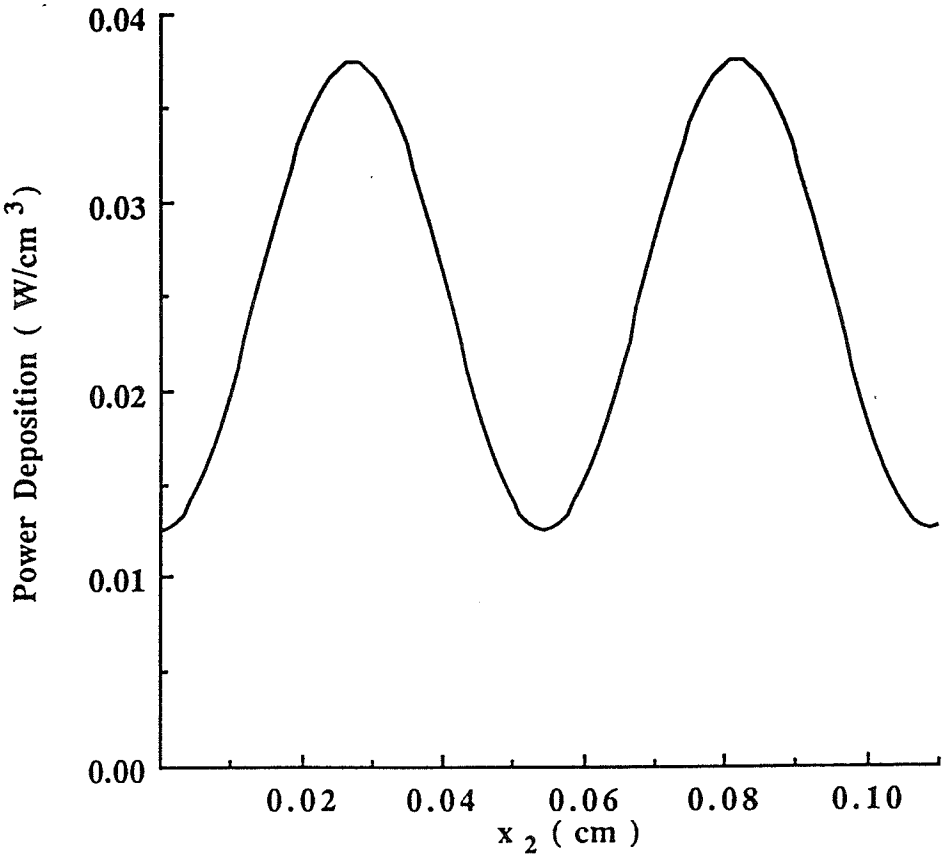

Figure 2b. Power deposition versus distance from the interface in the incident medium for zero bulk viscosity using Eq. (14); same as Nyborg's[18] plot.

These tests show that the theory presented in this paper provides solutions that agree with results previously reported for less general theories.

4. POWER DEPOSITION CALCULATION

The power deposition, P_L, was computed near muscle-bone and muscle-air interfaces directly without separating the intensity into shear and longitudinal components. Results obtained by this direct calculation were then compared to those obtained with the methods of Chan et al.[10] and Frizzell and Carstensen[12] for separation of energy into shear and longitudinal components at the interface. Cross-term intensities were attributed to shear and longitudinal waves based on the ratios of the magnitudes (Eq. (17)), after Chan et al.[10], and on the ratios of the squares of magnitudes (Eq. (18)), after Frizzell and Carstensen[12], of the respective potential coefficients.

$$I_{\text{refl.-long.}} = I_{\text{pure-refl.-long.}} + \frac{|L_R|}{|L_R| + |S_R|} I_{\text{unprimed cross term}} \tag{17a}$$

$$I_{\text{refl.-shear}} = I_{\text{pure-refl.-shear}} + \frac{|S_R|}{|L_R| + |S_R|} I_{\text{unprimed cross term}} \tag{17b}$$

$$I_{\text{trans.-long.}} = I_{\text{pure-trans.-long.}} + \frac{|L_T|}{|L_T| + |S_T|} I_{\text{primed cross term}} \tag{17c}$$

$$I_{\text{trans.-shear}} = I_{\text{pure-trans.-shear}} + \frac{|S_T|}{|L_T| + |S_T|} I_{\text{primed cross term}} \tag{17d}$$

$$I_{\text{refl.-long.}} = I_{\text{pure-refl.-long.}} + \frac{|L_R|^2}{|L_R|^2 + |S_R|^2} I_{\text{unprimed cross term}} \tag{18a}$$

$$I_{\text{refl.-shear}} = I_{\text{pure-refl.-shear}} + \frac{|S_R|^2}{|L_R|^2 + |S_R|^2} I_{\text{unprimed cross term}} \tag{18b}$$

$$I_{trans.-long.} = I_{pure-trans.-long.} + \frac{|L_T|^2}{|L_T|^2 + |S_T|^2} I_{primed\ cross\ term} \quad (18c)$$

$$I_{trans.-shear} = I_{pure-trans.-shear} + \frac{|S_T|^2}{|L_T|^2 + |S_T|^2} I_{primed\ cross\ term} \quad (18d)$$

The energies on the right-hand sides of Eqs. (17) and (18) are defined as follows, and are calculated at the origin of the coordinate system. Also, see Appendix A.

$I_{inc.}$ = pure incident term ($\Phi_I\Phi_I^*$ term) (19a)

$I_{pure-refl.-long.}$ = pure reflected longitudinal term ($\Phi_R\Phi_R^*$ term) (19b)

$I_{pure-refl.-shear}$ = pure reflected shear term (AA^* term) (19c)

$I_{pure-trans.-long.}$ = pure transmitted longitudinal term ($\Phi'\Phi'^*$ term) (19d)

$I_{pure-trans.-shear}$ = pure transmitted shear term ($A'A'^*$ term) (19e)

$I_{unprimed\ cross\ terms}$ = sum of cross terms in the incident (unprimed) medium (19f)

$I_{primed\ cross\ terms}$ = sum of cross terms in the transmitted (primed) medium (19g)

The power depositions as a function of distance from the interface were then calculated by applying the appropriate absorption coefficient to both shear and longitudinal waves and using ray tracing to determine the contribution from each wave at a particular distance. When only one kind of wave is propagating

in the +d direction in an unbounded medium, the intensity can be described by

$$I(d) = I_o\, e^{-2\alpha d} \tag{20a}$$

and the power deposition by

$$P_L(d) = 2\alpha I_o\, e^{-2\alpha d}, \tag{20b}$$

where I_o is the intensity at d = 0 and α is the absorption coefficient. In this simplified calculation, the power deposition due to each kind of wave is calculated as if that wave were the only one propagating, using the intensities computed in Eq. (17) or Eq. (18) at the origin of the coordinate system for each value of I_o and the appropriate absorption coefficient for α. The value of d depends on the distance from the interface (x_2) and on the real angles of incidence, reflection, and refraction (θ, ψ, θ', ψ') (see Fig. 1). These are not the real parts of the complex angles found in Eq. (10), but must be calculated from ratios of the x_1 and x_2 components of the intensities in Eq. (19). The distance d is calculated as follows. Because the incident wave is assumed to have infinite beamwidth, the values of x_1 and x_3 are taken to be zero without loss of generality. However, the rays contributing to the power deposition at each point along the $x_1 = x_3 = 0$ line are reflected from or transmitted through points on the interface (the $x_2 = 0$ plane) other than the origin of the coordinate system, where the energies in Eq. (19) were calculated. Figures 3a and 3b each show two rays representing the incident wave. One reaches the interface at the origin, and the other, which is reflected in Fig. 3a and transmitted in Fig. 3b, reaches

the interface at a point at which the value of x_1 is less than zero. The incident rays impinging on those reflection and transmission points are less attenuated than the incident ray whose intensity was calculated in Eq. (19a), since the latter traveled a distance d_1 farther and was more attenuated.

$$d_1 = -x_1 \sin\theta \tag{21}$$

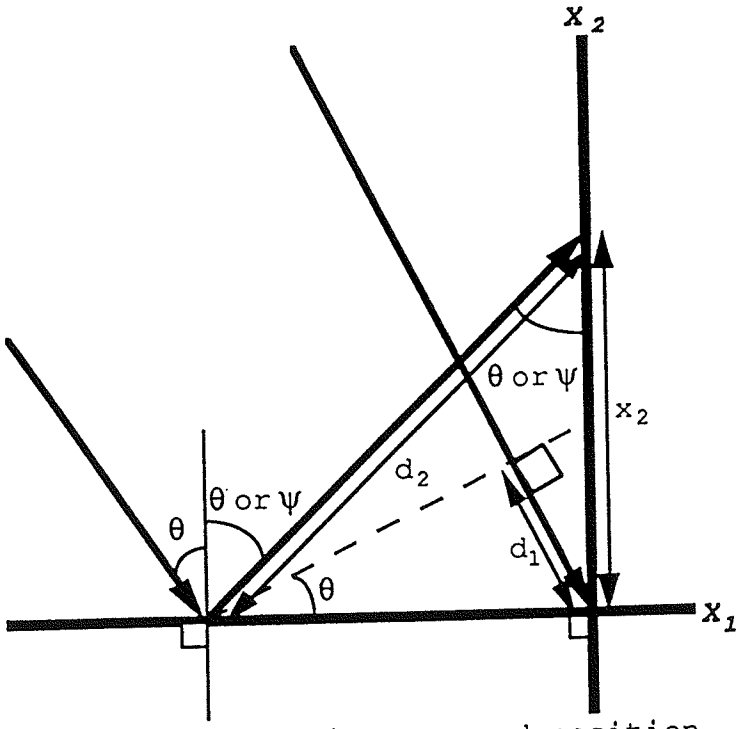

Figure 3a. Geometry for estimating power deposition. Bold lines with arrows at one end are rays representing incident and reflected waves. Thin lines with arrows at both ends indicate distances. Dashed lines represent phase fronts.

The distance d_2 and the value of x_1 in Fig. 3a is given by Eq. (22) for the case of the reflected longitudinal wave and by Eq. (23) for the case of the reflected shear wave.

$$d_2 = x_2 \sec\theta \tag{22a}$$

$$\tan\theta = \frac{-x_1}{x_2} \tag{22b}$$

$$d_2 = x_2 \sec\psi \tag{23a}$$

$$\tan\psi = \frac{-x_1}{x_2} \tag{23b}$$

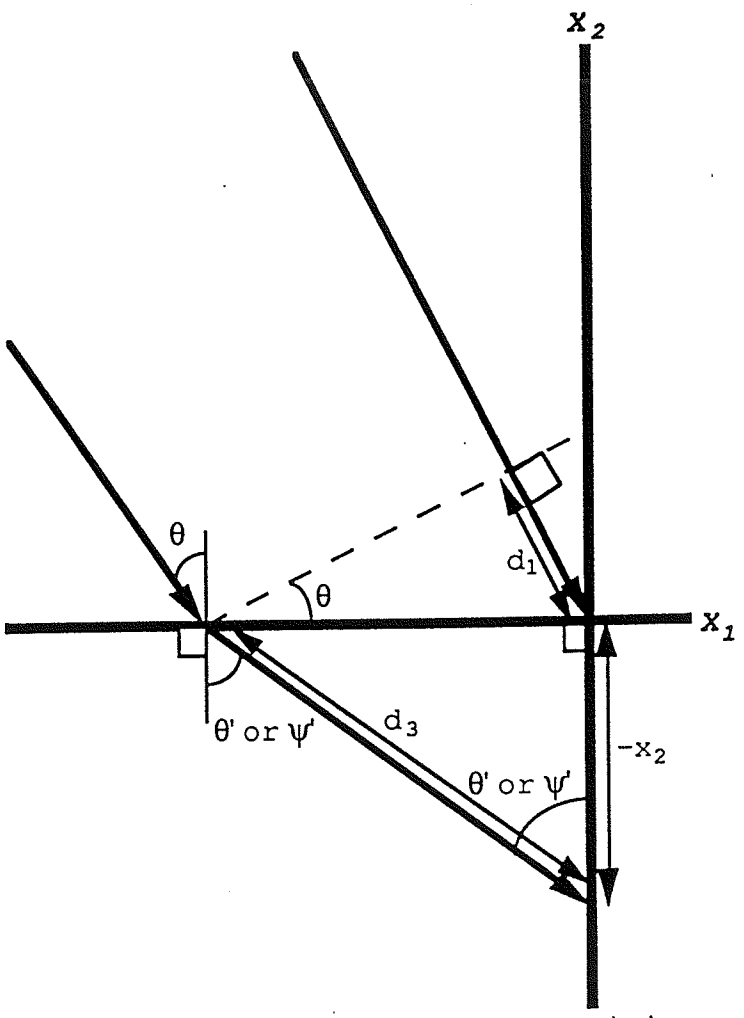

Figure 3b. Geometry for estimating power deposition. Bold lines with arrows at one end are rays representing incident and transmitted waves. Thin lines with arrows at both ends indicate distances. Dashed lines represent phase fronts.

The distance d_3 and the value of x_1 in Fig. 3b are given by Eq. (24) for the case of the transmitted longitudinal wave and by Eq. (25) for the case of the transmitted shear wave.

$$d_3 = x_2 \sec\theta' \tag{24a}$$

$$\tan\theta' = \frac{x_1}{x_2} \tag{24b}$$

$$d_3 = x_2 \sec\psi' \tag{25a}$$

$$\tan\psi = \frac{x_1}{x_2} \tag{25b}$$

Then the contributions from the wave components calculated with Eq. (20b) were summed to get the total power deposition as a function of distance from the interface.

power deposition in the unprimed medium =

$$2\alpha_L(I_{inc.}(@x_1 = x_2 = 0)\exp[2\alpha_L x_2 \cos\theta] + I_{refl.-long.}(@x_1 = x_2 = 0)\exp[-2\alpha_L x_2 \cos\theta]) + 2\alpha_S I_{refl.-shear}(@x_1 = x_2 = 0)\exp[2x_2(\alpha_L \sin\theta\tan\psi - \alpha_S' \sec\psi)] \tag{26a}$$

power deposition in the primed medium =

$$2\alpha_L' I_{trans.-long.}(@x_1 = x_2 = 0)\exp[2x_2(\alpha_L \sin\theta\tan\theta' - \alpha_L' \sec\theta')] + 2\alpha_S' I_{trans.-shear}(@x_1 = x_2 = 0)\exp[2x_2(\alpha_L \sin\theta\tan\psi' - \alpha_S' \sec\psi')] \tag{26b}$$

The results are plotted in Fig. 4 as a function of x_2 for an incident intensity of 1 W/cm^2 and incident angles of 0°, 30°, and 60°. Table 2 lists the properties used.

Table 2. Properties of tissues at 2 MHz used for mode conversion computations.

	Muscle	Air	Bone
c_L (cm/s)	154,000[17,18]	34,400[20]	336,000[17,18]
α_L (cm^{-1})	0.15[17,18]	0.8[20]	2.5[17,18]
c_S (cm/s)	2,200[10]	2,000*	179,000[17,18]
α_S (cm^{-1})	5,000[10]	6,500*	4.0[17,18]
K_L (cm^{-1})	81.6 - j0.15	365 - j0.8	37.4 - j2.5
K_S (cm^{-1})	5,710 - j5,000	6,280 - j6,500	70.2 - j4.0
ρ (g/cm^3)	1.1	0.0012	1.7

The superscripted numbers refer to the reference used.
* The shear properties of air were calculated based on its shear viscosity.

Results obtained using either method of separating intensities do not show the spatially oscillating nature of the power deposition that is exhibited by P_L, the directly calculated power deposition. It is seen in Figs. 4a, 4c, and 4e that within the muscle, results using Chan's method approximate the spatial average of P_L. Results from Frizzell and Carstensen's method were higher than the spatial average. However, Figs. 4d and 4f show that within the bone the results from Chan's method for oblique incidence are not a good approximation to P_L, especially at large angles of incidence. Results from Frizzell and Carstensen's method were a slightly better approximation.

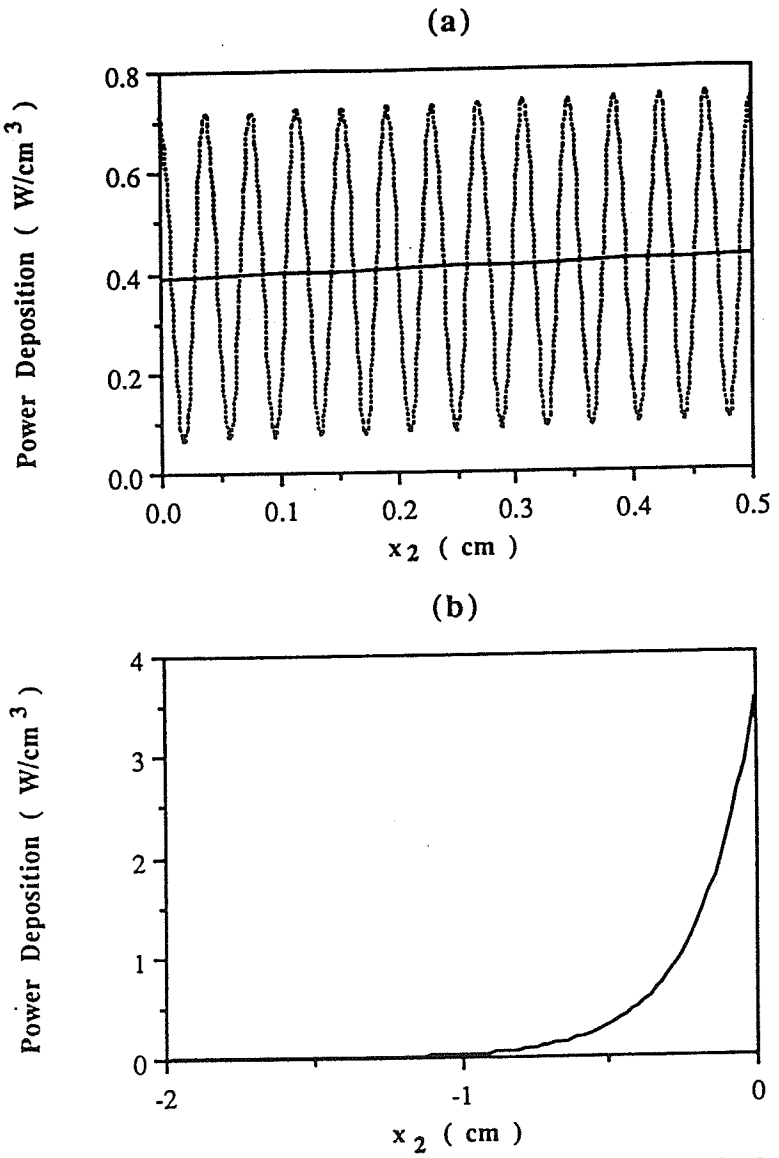

Figure 4. Results from calculations of power deposition P_L in muscle (a) and in bone (b) at 0° angle of incidence using Eq. (14) (- - -), and dividing cross-term intensities as done by Chan et al.[10] (———).

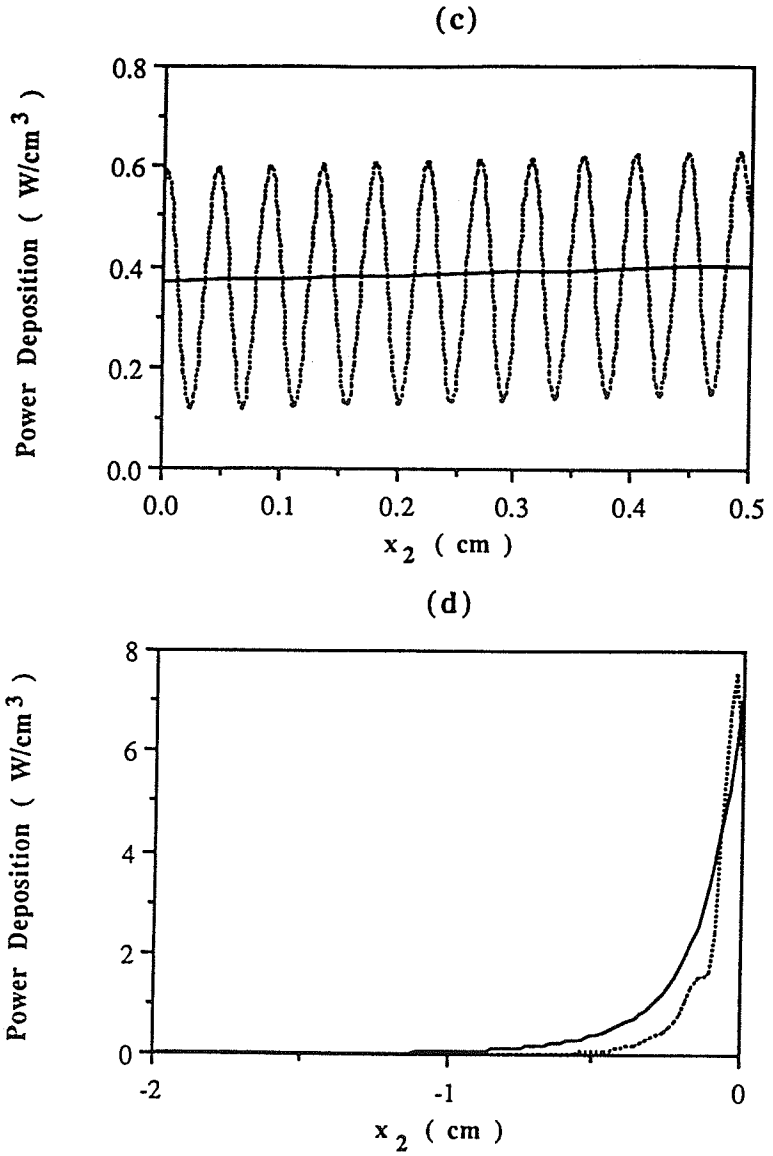

Figure 4. Results from calculations of power deposition P_L in muscle (c) and in bone (d) at 30° angle of incidence using Eq. (14) (- - -), and dividing cross-term intensities as done by Chan et al.[10] (———).

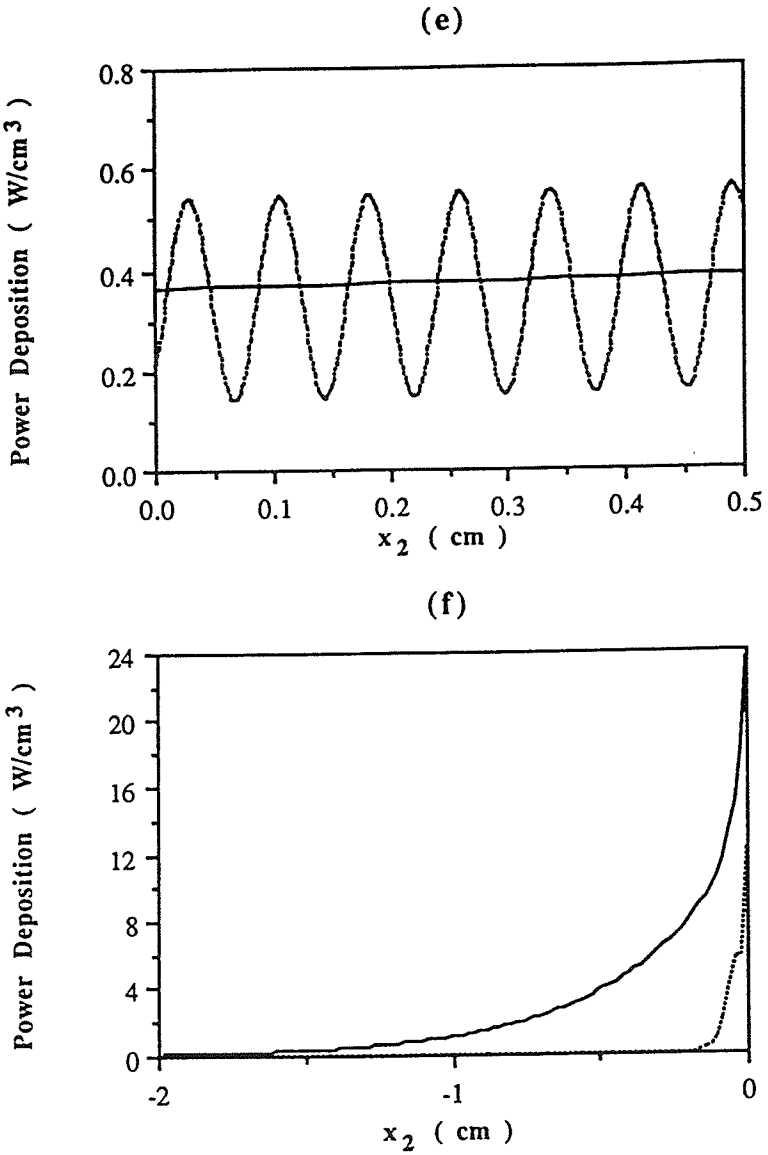

Figure 4. Results from calculations of power deposition P_L in muscle (e) and in bone (f) at 60° angle of incidence using Eq. (14) (- - -), and dividing cross-term intensities as done by Chan et al.[10] (———).

Since power deposition calculated using this method was not in particularly good agreement with P_L, it seems that these methods of classifying the energies as shear or longitudinal are not very useful. In the next chapter a different method of studying the effect of shear waves on power deposition will be described.

5. ISOLATION OF SHEAR WAVE EFFECTS

Another way of studying the effect of shear waves on power deposition is to compare the intensity and the power deposition in media which are the same except for their ability to support shear waves. Instead of solving a new set of equations where shear waves are not allowed in one or both media, shear waves were virtually eliminated by changing the shear absorption coefficient to an arbitrarily large value.

$$\alpha_S \text{ and/or } \alpha_S' = 10^8 \text{ cm}^{-1} \tag{27}$$

As shown by Eq. (2b), a medium with zero shear stiffness and zero shear viscosity has an infinite value for K_S, that is, $\alpha_S = \infty$ and $c_S = 0$. However, shear waves are eliminated just by letting α_S approach an infinite value. As shown in Appendix B, all of the terms in the expressions for power deposition (found in Appendix A) which involve shear waves, that is, which involve vector potentials, go to zero in the limit that the shear absorption coefficient goes to infinity. A material in which shear waves have been eliminated in this manner will be referred to as "shearless."

Power deposition was computed as a function of angle of incidence immediately adjacent to the interface for muscle-bone and muscle-air interfaces (incident wave in muscle) as shown in Figs. 5 and 6, respectively. In each figure four cases are plotted: a calculation using measured values for the shear absorption coefficients and three calculations using the specified

large value for α_S, α_S', or both to make the media each individually or both "shearless."

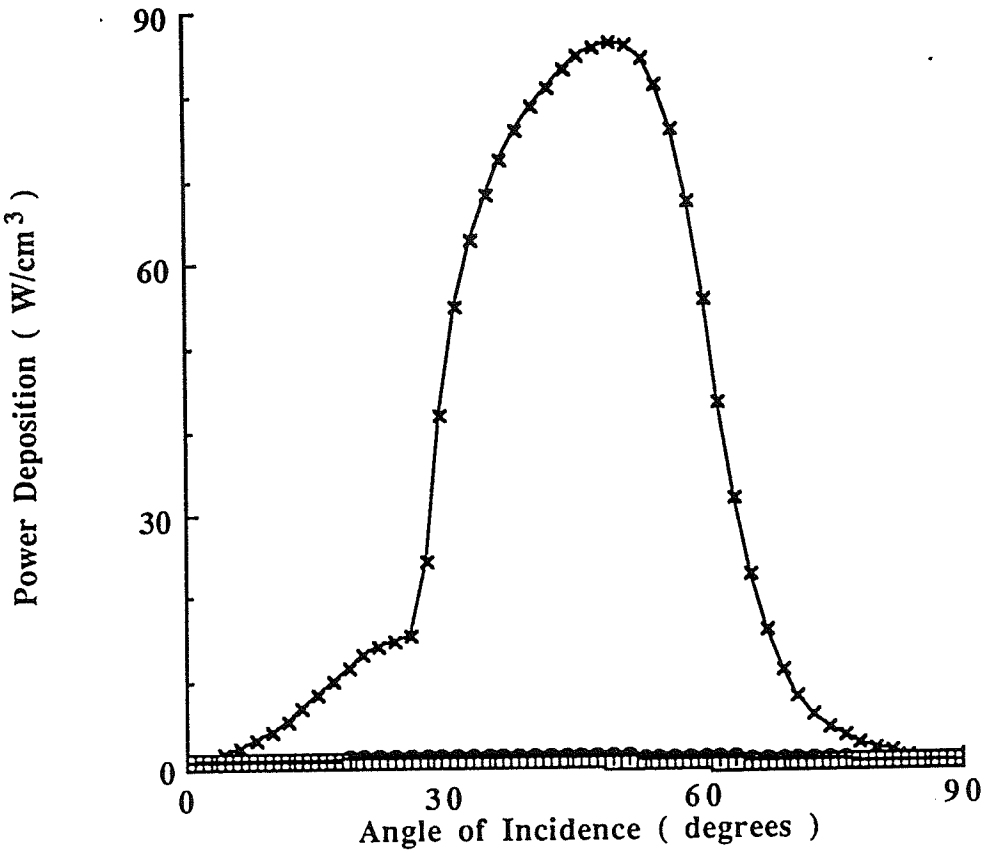

Figure 5a. Power deposition versus angle of incidence at $x_2 = 10^{-5}$ cm (in the "muscle") for a muscle-bone interface (X), a muscle-"shearless" bone interface (O), a "shearless" muscle-bone interface (□), and a "shearless" muscle-"shearless" bone interface (+).

It is clear from Fig. 5a that substituting "shearless" muscle or "shearless" bone or making both media "shearless" immensely reduces the power deposition in the muscle. Thus, shear waves do contribute significantly to power deposition in soft tissue

immediately adjacent to an interface with another medium which supports shear waves.

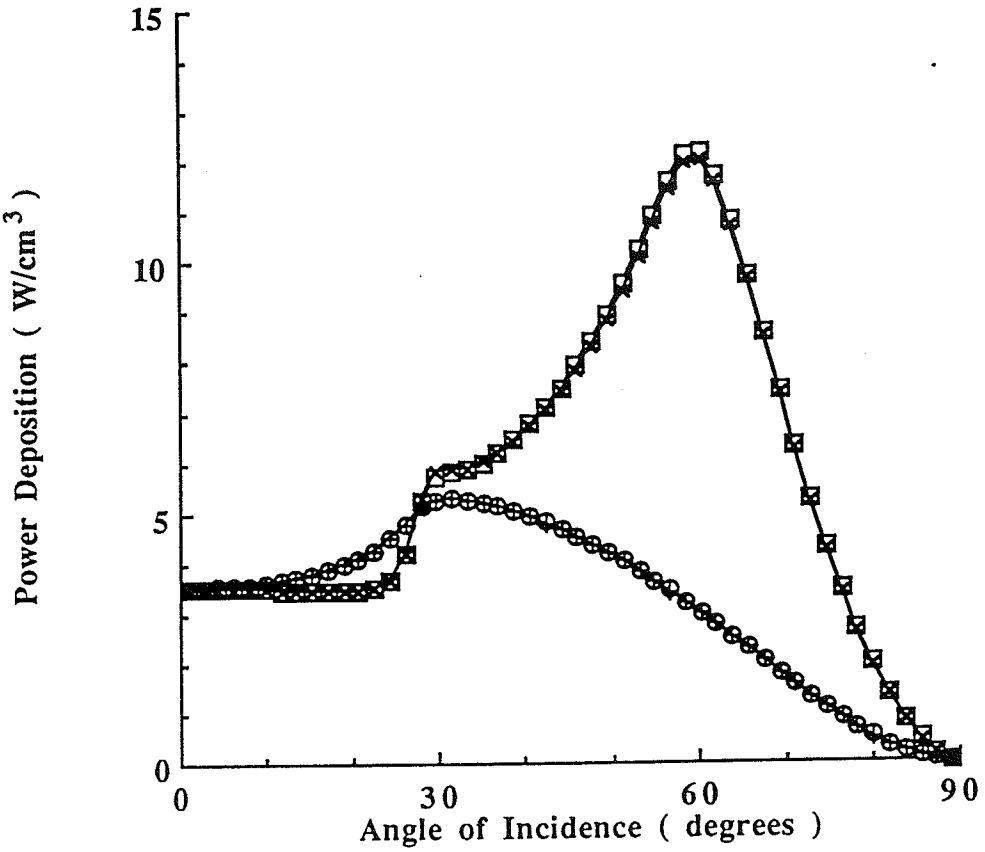

Figure 5b. Power deposition versus angle of incidence at $x_2 = -10^{-5}$ cm (in the "bone") for a muscle-bone interface (X), a muscle-"shearless" bone interface (O), a "shearless" muscle-bone interface (□), and a "shearless" muscle-"shearless" bone interface (+).

In the bone, power deposition is significantly smaller for a muscle-"shearless" bone interface than for a muscle-bone interface, as expected, but the "shearless" muscle-bone case is indistinguishable from the muscle-bone case (Fig. 5b). Thus,

existence of shear waves in the muscle has no effect on power deposition in the bone.

For comparison it is interesting to examine an interface between muscle and air with the incident wave in the muscle (Fig. 6). When the air is "shearless," the power deposition is not appreciably smaller in the muscle than it is for a muscle-air interface (Fig. 6a), but, as might be expected, is also noticeably smaller in the air (Fig. 6b). For interfaces between "shearless" muscle and air or "shearless" muscle and "shearless" air, the power deposition is significantly smaller in both media. This again shows that the contribution of shear waves to power deposition for oblique incidence in soft tissue, immediately adjacent to the interface, is significant.

Note that the power deposition in the muscle immediately adjacent to the interface is very low at all angles of incidence and near zero at normal incidence because the air interface approximates a free surface, where the acoustic pressure and the power deposition would be zero.

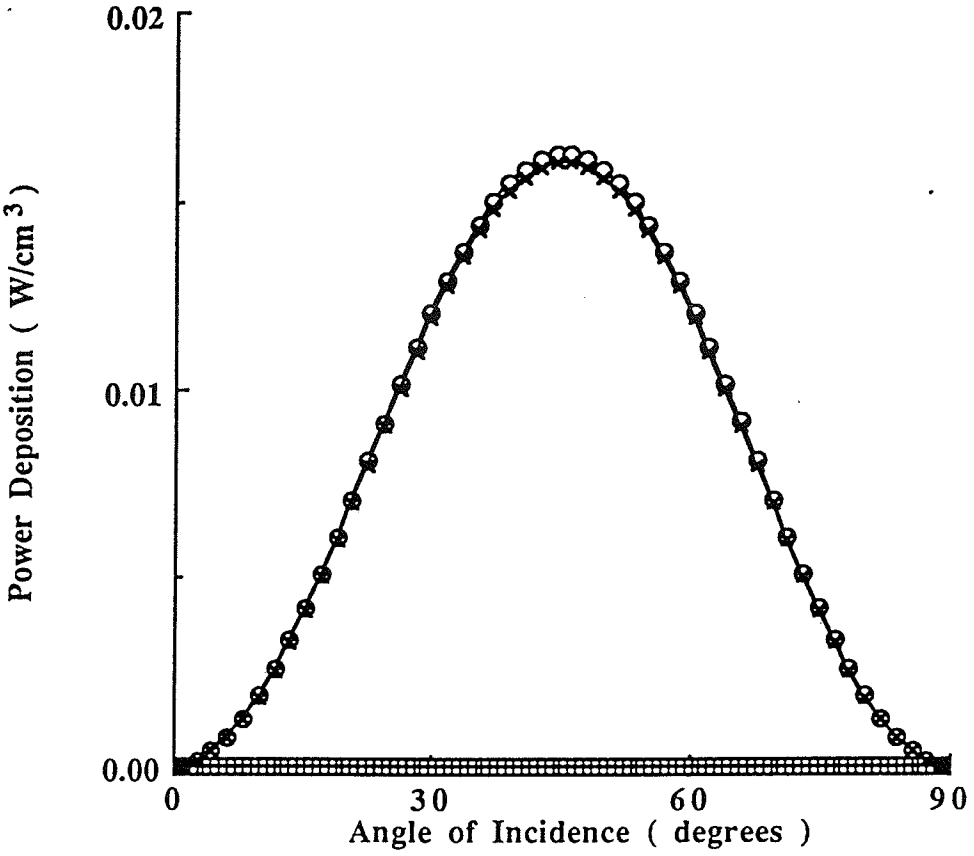

Figure 6a. Power deposition versus angle of incidence at $x_2 = 10^{-5}$ cm (in the "muscle") for a muscle-air interface (X), a muscle-"shearless" air interface (O), a "shearless" muscle-air interface (□), and a "shearless" muscle-"shearless" air interface (+).

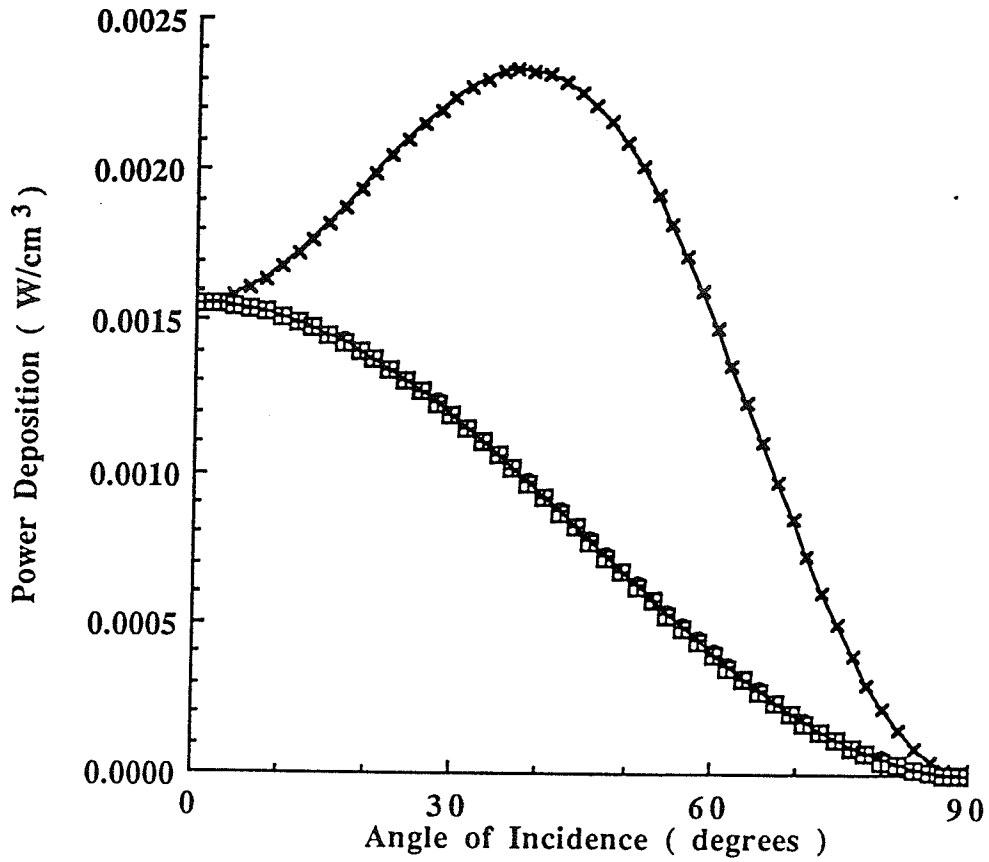

Figure 6b. Power deposition versus angle of incidence at $x_2 = -10^{-5}$ cm (in the air) for a muscle-air interface (X), a muscle-"shearless" air interface (O), a "shearless" muscle-air interface (□), and a "shearless" muscle-"shearless" air interface (+).

In Figure 7, the power depositions are plotted versus distance from the interface at angles of incidence of 30° and 60° for the four different types of muscle-bone interfaces. Figures 7a and 7b are both plots of power deposition within the muscle for an incident angle of 30°.

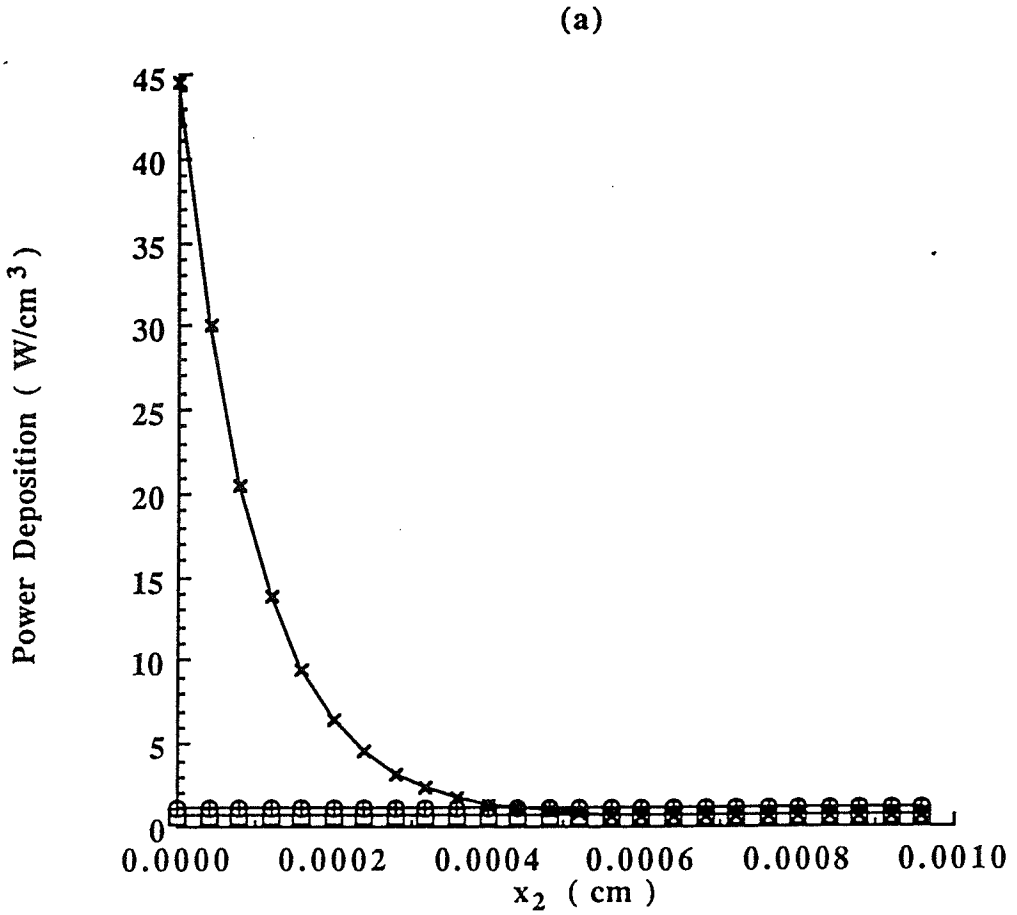

Figure 7a. Power deposition versus distance from the interface for a muscle-bone interface (X), a muscle-"shearless" bone interface (O), a "shearless" muscle-bone interface (□), and a "shearless" muscle-"shearless" bone interface (+), at $\theta = 30°$ in the "muscle."

Figure 7a shows that the contribution to P_L from the shear wave has disappeared at approximately 5 μm from the interface. Figure 7b shows the behavior of P_L at distances greater than 5 μm from the interface. It can be seen clearly in Fig. 7b that the results for the muscle-bone and the "shearless" muscle-bone interfaces are indistinguishable at distances greater than a few micrometers from the interface.

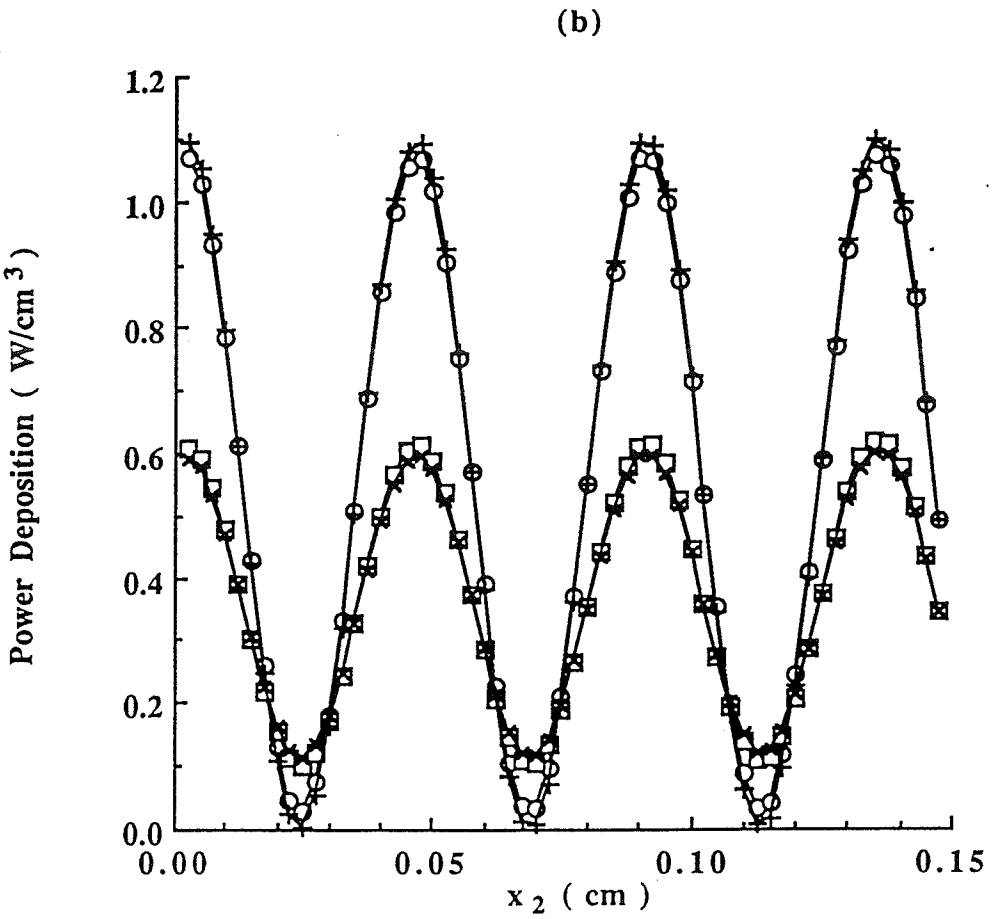

Figure 7b. Power deposition versus distance from the interface for a muscle-bone interface (X), a muscle-"shearless" bone interface (O), a "shearless" muscle-bone interface (□), and a "shearless" muscle-"shearless" bone interface (+), at $\theta = 30°$ in the "muscle."

A similar result was obtained for shear waves in muscle at a muscle-air interface. Also, the results for the muscle-"shearless" bone and the "shearless" muscle-"shearless" bone interfaces are indistinguishable, as noted previously.

Figure 7c shows the power deposition within bone for an angle of incidence of 30°. Here it can also be seen that the results for muscle-bone and "shearless" muscle-bone are indistinguishable

as are the results for muscle-"shearless" bone and "shearless" muscle-"shearless" bone. Thus, the existence of shear waves in the muscle has no effect on power deposition within the bone.

(c)

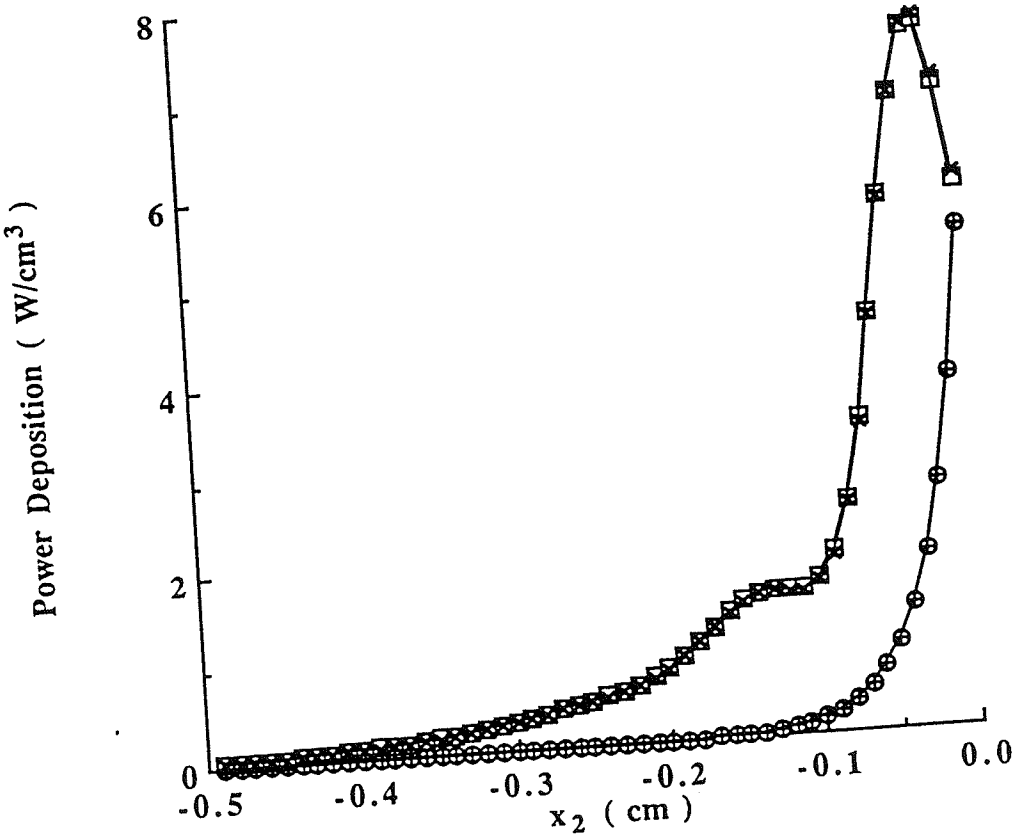

Figure 7c. Power deposition versus distance from the interface for a muscle-bone interface (X), a muscle-"shearless" bone interface (O), a "shearless" muscle-bone interface (□), and a "shearless" muscle-"shearless" bone interface (+) at $\theta = 30°$ in the "muscle."

Figures 7d, 7e, and 7f show that results at an incident angle of 60° are qualitatively similar to those for 30° angle of incidence.

(d)

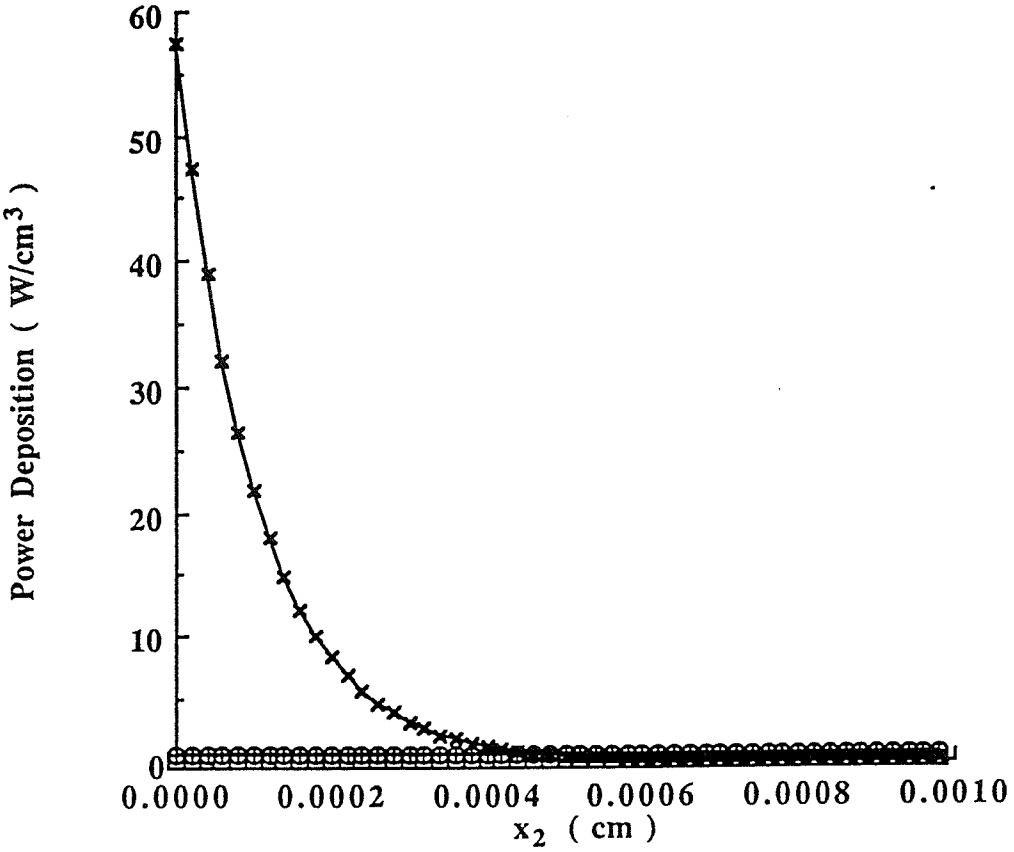

Figure 7d. Power deposition versus distance from the interface for a muscle-bone interface (X), a muscle-"shearless" bone interface (O), a "shearless" muscle-bone interface (□), and a "shearless" muscle-"shearless" bone interface (+), $\theta = 60°$ in the "muscle."

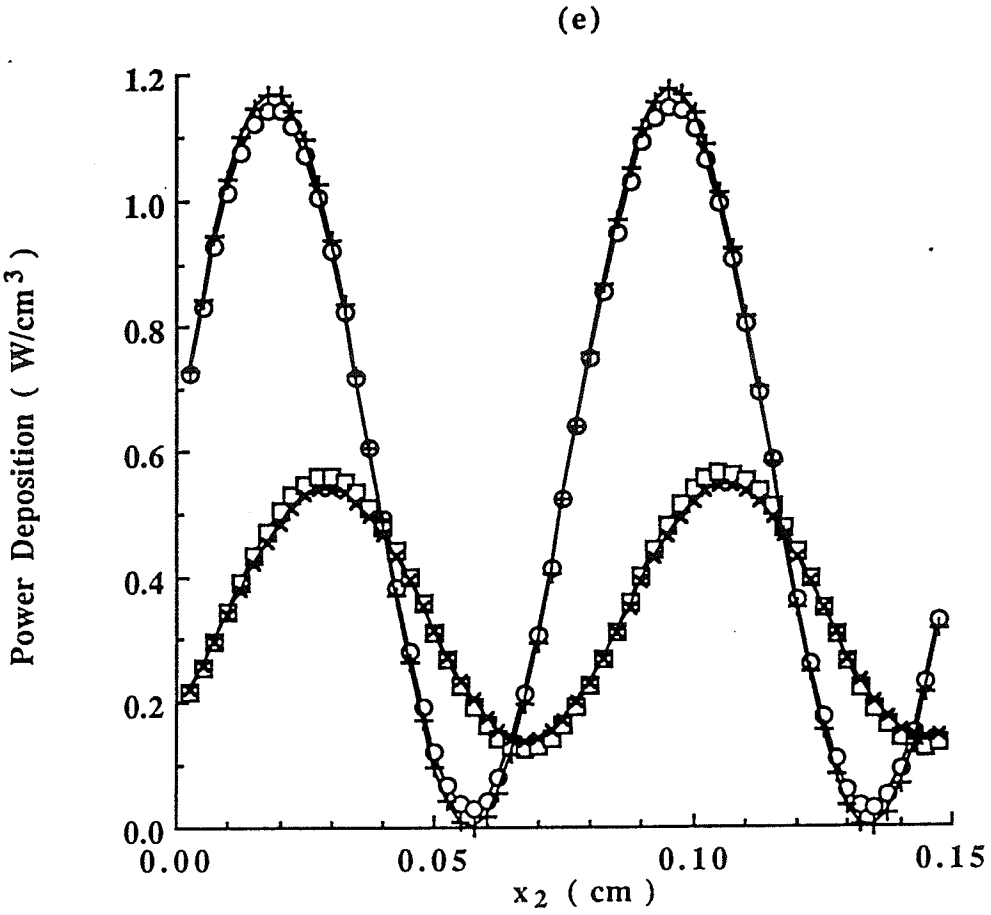

Figure 7e. Power deposition versus distance from the interface for a muscle-bone interface (X), a muscle-"shearless" bone interface (O), a "shearless" muscle-bone interface (□), and a "shearless" muscle-"shearless" bone interface (+), at $\theta = 60°$ in the "muscle."

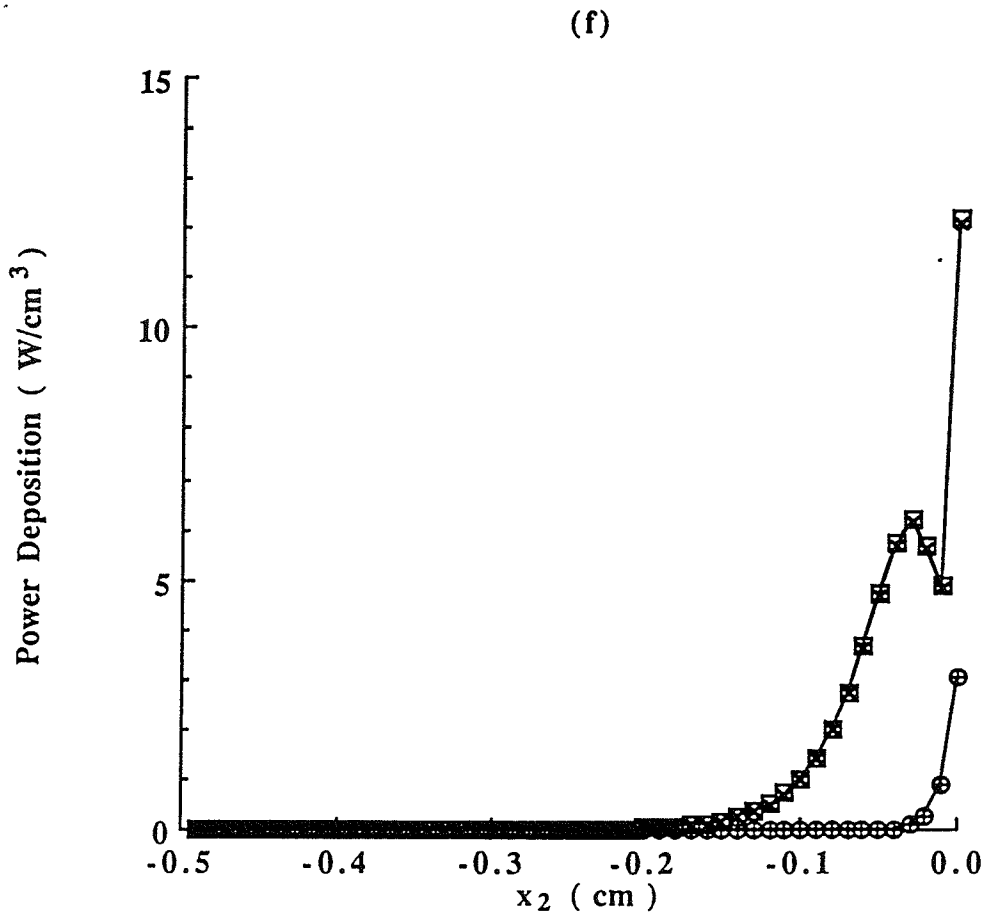

Figure 7f. Power deposition versus distance from the interface for a muscle-bone interface (X), a muscle-"shearless" bone interface (O), a "shearless" muscle-bone interface (□), and a "shearless" muscle-"shearless" bone interface (+), at $\theta = 60°$ in the "bone."

The results discussed to this point show that shear waves in muscle contribute significantly to power deposition only within a few micrometers of the interface. It is desirable to determine the contribution of these shear waves to the temperature rise near the interface. A method of estimating their contribution is described in the next chapter.

6. ESTIMATE OF SHEAR WAVE CONTRIBUTION TO TEMPERATURE RISE

In the previous chapter, calculations indicated that shear waves were important to power deposition only very near to the interface. The next step is to find the effect of shear waves on temperature rise, a measurable consequence of power deposition, near the interface. To estimate shear wave contribution to temperature rise at the interface, P_L was integrated from $x_2 = -1$ cm to $x_2 = 1$ cm to determine the total energy deposited within 1 cm of the interface per unit area of the interface. A distance of 1 cm was chosen to be large enough to include all of the contributions from shear waves in muscle and bone. Yet, 1 cm is small enough that the energy deposited within that distance will, by conduction, contribute to the temperature rise near the interface after several minutes. The results for the integrated power deposition for 1 cm of bone and 1 cm of muscle are plotted separately as functions of angle of incidence in Figs. 8a and 8b to provide more detail. It is clear from an examination of these results that the existence of shear waves in the muscle makes a negligible contribution to the total energy deposited within 1 cm of the interface and therefore to the temperature rise near the interface.

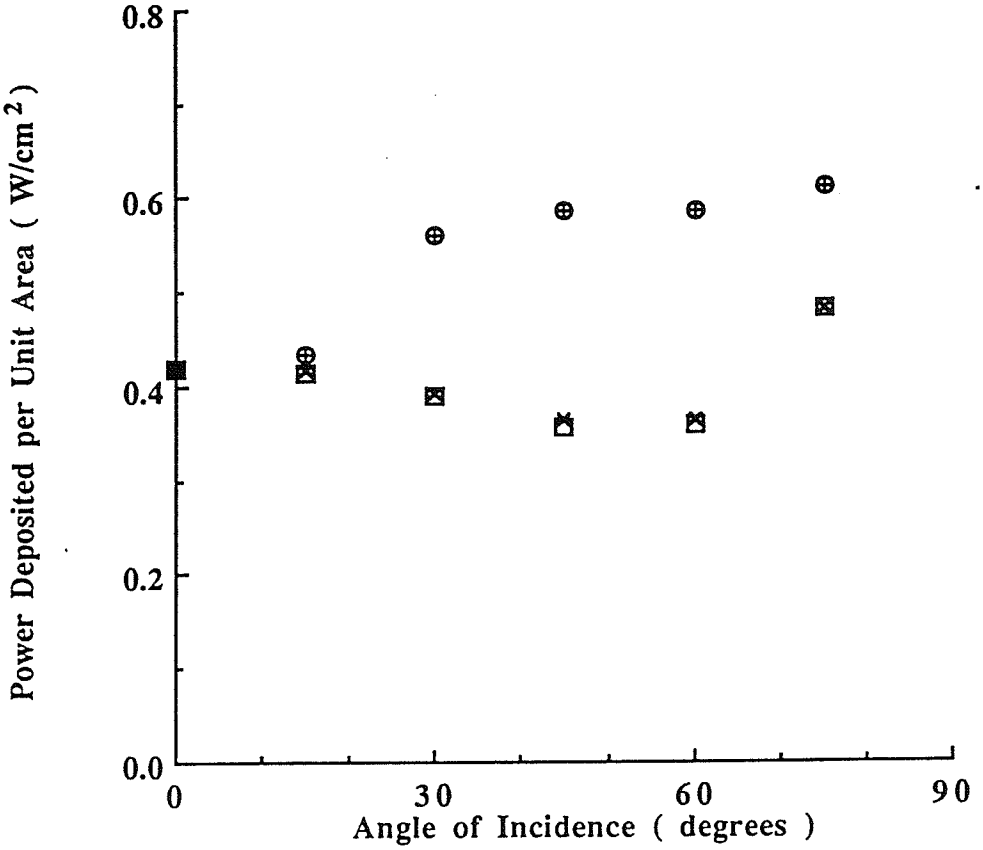

Figure 8a. Power deposition for a muscle-bone interface (X), a muscle-"shearless" bone interface (O), a "shearless" muscle-bone interface (□), and a "shearless" muscle-"shearless" bone interface (+) at $x_1 = 0$ numerically integrated over x_2 from 10^{-10} cm to 1 cm in the "muscle". Step size is 10^{-2} cm, except for distances from the interface between 10^{-10} and 10^{-3} cm, where the step size is 10^{-5} cm.

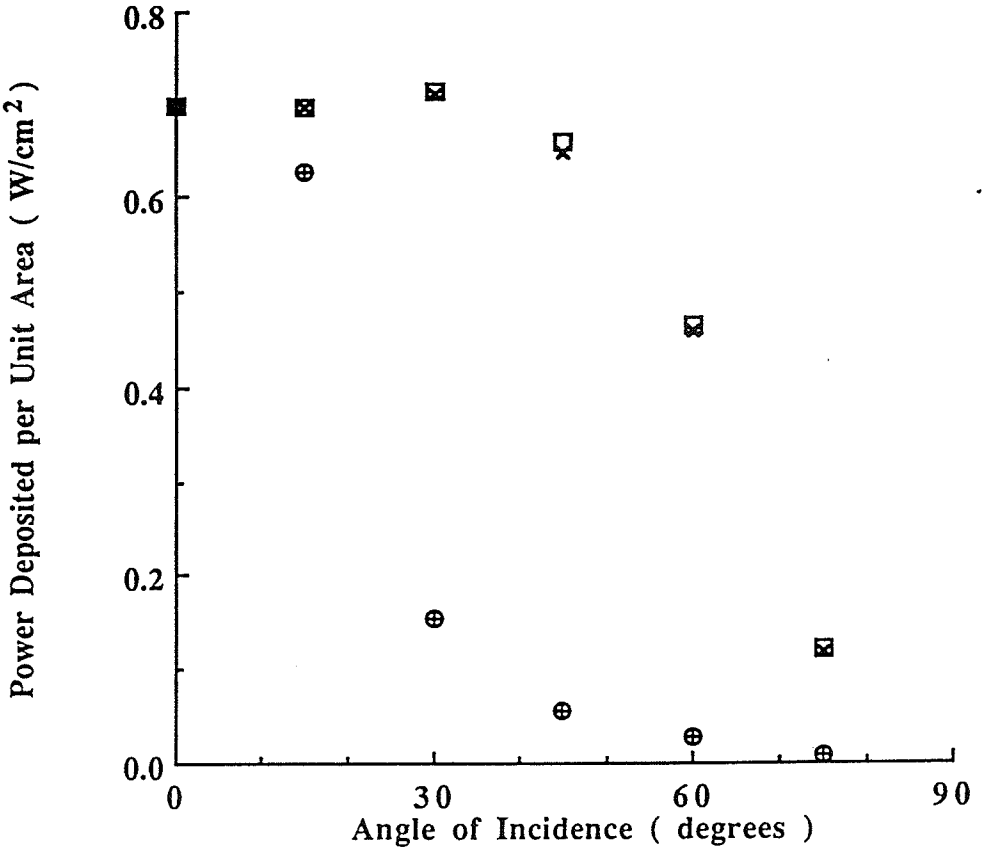

Figure 8b. Power deposition for a muscle-bone interface (X), a muscle-"shearless" bone interface (O), a "shearless" muscle-bone interface (□), and a "shearless" muscle-"shearless" bone interface (+) at $x_1 = 0$ numerically integrated over x_2 from -10^{-10} cm to -1 cm in the "bone". Step size is 10^{-2} cm.

It is apparent from Fig. 8b that the integrated power deposition in bone does not significantly increase with angle of incidence, as might be erroneously concluded intuitively, based on conversion of energy to more highly absorbed shear waves. In fact, the integrated power deposition begins to decrease with angles of incidence greater than approximately 35°, apparently due to greater reflection of energy at the bone interface. Yet, shear

waves in the bone do contribute significantly to heating because the integrated power deposition for "shearless" bone begins to decrease rapidly with angles of incidence greater than approximately 15°.

Results at an interface between muscle and air also indicate that shear waves in the muscle made a negligible contribution to the integrated power deposition near the interface. This confirms the result of Filipczynski[11], who used a less general theory to show that shear waves in the soft tissue at a gas interface provide a negligible contribution to temperature rise compared to longitudinal waves.

7. CONCLUSIONS AND SUGGESTIONS FOR FUTURE STUDY

The results of this study show that the assignment of energy to shear and longitudinal waves as done by Chan et al.[10] and by Frizzell and Carstensen[12] yields an inaccurate representation of power deposition. The details of the spatial resolution are lost, and the magnitude is incorrect in many instances compared to the true power deposition as determined by direct calculation without consideration of whether the energy is in a shear or longitudinal wave.

Shear waves in bone contribute significantly to heating, but shear waves in soft body tissues such as muscle make a negligible contribution to heating at tissue interfaces. This is a quantitative validation of the assumption by Chan et al.[10], and confirms the results of Filipczynski[11] for interfaces with gas, that shear waves in soft tissues such as muscle can be ignored in studies of interfacial heating.

The integrated power deposition, which is related to temperature rise, in the bone does not significantly increase with angle of incidence, as might erroneously be concluded intuitively, based on conversion of energy to more highly absorbed shear waves. The integrated power deposition in the bone begins to decrease with angles of incidence greater than approximately 35°, apparently due to greater reflection of energy at the bone interface.

The results of this work should be verified and extended by considering other geometries and by using the bioheat equation to calculate the actual temperature rise at interfaces. An important case to be studied is cylindrical geometry, which would be a better model of a muscle-bone interface, particularly for fetal ultrasound exposures, where the bone is not large compared to the beamwidth. Such a study would require the use of a cylindrical coordinate system and Bessel functions. The results of Chapter 6 can be verified by using the bioheat equation to make a better estimate of the temperature rise. Decisions involved in that study include choosing boundary conditions for the temperature profile and considering the effect of blood perfusion.

APPENDIX A: INTENSITY AND POWER DEPOSITION EXPRESSIONS

The following are the intensity equations developed in L. A. Frizzell's thesis, "Ultrasonic Heating of Tissues" from Eq. (12)[12]. A prime (') symbol denotes the primed or transmitting medium. A subscript 1 refers to the direction parallel to the interface; a subscript 2 refers to the direction perpendicular to the interface. The complex Lamé constant λ is defined in Eq. (A1).

$$\lambda = B - \frac{2}{3}\mu. \tag{A1}$$

An asterisk (*) denotes complex conjugate. The potentials Φ_I, Φ_R, A, Φ', and A' and other symbols are defined in the body of the paper.

$$\begin{aligned} I_1 = \frac{\omega}{2} \mathrm{Re}\{ & (\lambda + 2\mu) K_L \sin\theta \ (\Phi_I\Phi_I^* + \Phi_R\Phi_R^*) \\ & + (2\mu K_S \sin\psi \cos\psi \cos^*\psi + \mu K_S \sin^*\psi \ (\sin^2\psi - \cos^2\psi)) \ AA^* \\ & + (\lambda K_L \sin\theta + 2\mu K_L \sin\theta \ (\sin^2\theta - \cos^2\theta)) \ (\Phi_I\Phi_R^* + \Phi_I^*\Phi_R) \\ & + ((\lambda + 2\mu) K_L \sin^2\theta \cos^*\psi + \lambda K_L \cos^2\theta \cos^*\psi + 2\mu K_L \sin\theta \cos\theta \sin^*\psi) \ \Phi_I A^* \\ & + ((\lambda + 2\mu) K_L \sin^2\theta \cos^*\psi + \lambda K_L \cos^2\theta \cos^*\psi - 2\mu K_L \sin\theta \cos\theta \sin^*\psi) \ \Phi_R A^* \\ & + (2\mu K_S \sin\psi \cos\psi \sin\theta + \mu K_S \cos\theta \ (\sin^2\psi - \cos^2\psi)) \ \Phi_I^* A \\ & + (2\mu K_S \sin\psi \cos\psi \sin\theta - \mu K_S \cos\theta \ (\sin^2\psi - \cos^2\psi)) \ \Phi_R^* A \} \end{aligned}$$

$$\begin{aligned} I_2 = \frac{\omega}{2} \mathrm{Re}\{ & (\lambda + 2\mu) K_L \cos\theta \ (\Phi_R\Phi_R^* - \Phi_I\Phi_I^*) \\ & + (2\mu K_S \sin\psi \sin^*\psi \cos^*\psi - \mu K_S \cos^*\psi \ (\sin^2\psi - \cos^2\psi)) \ AA^* \end{aligned}$$

$$+ (\lambda K_L \cos\theta + 2\mu K_L \cos\theta\ (\cos^2\theta - \sin^2\theta))\ (\Phi_I\Phi_R^* - \Phi_I^*\Phi_R)$$

$$+ (-(\lambda + 2\mu)K_L \cos^2\theta \sin^*\psi - \lambda K_L \sin^2\theta \sin^*\psi - 2\mu K_L \sin\theta \cos\theta \cos^*\psi)\ \Phi_I A^*$$

$$+ (-(\lambda + 2\mu)K_L \cos^2\theta \sin^*\psi - \lambda K_L \sin^2\theta \sin^*\psi + 2\mu K_L \sin\theta \cos\theta \cos^*\psi)\ \Phi_R A^*$$

$$+ (2\mu K_S \sin\psi \cos\psi \cos\theta - \mu K_S \sin\theta\ (\sin^2\psi - \cos^2\psi))\ \Phi_I^* A$$

$$+ (-2\mu K_S \sin\psi \cos\psi \cos\theta - \mu K_S \sin\theta\ (\sin^2\psi - \cos^2\psi))\ \Phi_R^* A \}$$

$$I_1' = \frac{\omega}{2} \mathrm{Re}\{ (K_L'(\lambda' + 2\mu') \sin^*\theta' \sin^2\theta' + \lambda' K_L' \sin^*\theta' \cos^2\theta' + 2\mu' K_L' \sin\theta' \cos\theta' \cos^*\theta')\ \Phi'\Phi'^*$$

$$+ (2\mu' K_S' \sin\psi' \cos\psi' \cos^*\psi' - \mu' K_S' \sin^*\psi' \cos^2\psi' + \mu' K_S' \sin^*\psi' \sin^2\psi')\ A'A'^*$$

$$+ (-(\lambda' + 2\mu')K_L' \sin^2\theta' \cos^*\psi' - \lambda' K_L' \cos^2\theta' \cos^*\psi' + 2\mu' K_L' \sin\theta' \cos\theta' \sin^*\psi')\ \Phi'A'^*$$

$$+ (-2\mu' K_S' \sin\psi' \cos\psi' \sin^*\theta' + \mu' K_S' \cos^*\theta' (\sin^2\psi' - \cos^2\psi'))\ \Phi'^*A' \}$$

$$I_2' = \frac{\omega}{2} \mathrm{Re}\{ (-2\mu' K_L' \sin\theta' \cos\theta' \sin^*\theta' - (\lambda' + 2\mu')K_L' \cos^*\theta' \cos^2\theta' - \lambda' K_L' \cos^*\theta' \sin^2\theta')\ \Phi'\Phi'^*$$

$$+ (\mu' K_S' \cos^*\psi' (\sin^2\psi' - \cos^2\psi') - 2\mu' K_S' \sin\psi' \sin^*\psi' \cos\psi')\ A'A'^*$$

$$+ (2\mu' K_L' \sin\theta' \cos\theta' \cos^*\psi' - (\lambda' + 2\mu')K_L' \cos^2\theta' \sin^*\psi' - \lambda' K_L' \sin^2\theta' \sin^*\psi')\ \Phi'A'^*$$

$$+ (-\mu' K_S' \sin^*\theta' (\sin^2\psi' - \cos^2\psi') - 2\mu' K_S' \sin\psi' \cos\psi' \cos^*\theta')\ \Phi'^*A' \}$$

The following are the equations for the power deposition derived from the above intensity equations using Eq. (14).

$$P_L = \frac{\omega}{2} [|K_L|^2 \, \mathrm{Im}\{\lambda + 2\mu\} \, (|\Phi_I|2 + |\Phi_R|2)$$

$$- |K_S|^2 \, \mathrm{Im}\{\mu\} \, |A|^2 \cosh(4 \, \mathrm{Im}\{\psi\})]$$

$$- 2\omega \, \mathrm{Im}\{\mu\} \, [\mathrm{Re}\{K_L K_S^* (\cos\theta \cos^*\psi - \sin\theta \sin^*\psi) \, (\cos\theta \sin^*\psi + \sin\theta \cos^*\psi) \, \Phi_I A^*\}$$

$$+ \mathrm{Re}\{K_L K_S^* (\cos\theta \cos^*\psi + \sin\theta \sin^*\psi) \, (\cos\theta \sin^*\psi - \sin\theta \cos^*\psi) \, \Phi_R A^*\}]$$

$$+ \omega |K_L|^2 \, \mathrm{Im}\{\lambda + 2\mu(1 - 2\sin^2\theta)^2\} \, \mathrm{Re}\{\Phi_I \Phi_R^*\}$$

$$P_L' = \frac{\omega}{2} [|K_L'|^2 \, \mathrm{Im}\{\lambda' + 2\mu' \cosh^2(2 \, \mathrm{Im}\{\psi'\})\} \, |\Phi'|^2 - |K_S'|^2 \, \mathrm{Im}\{\mu'\} \, |A'|^2 \cosh(4 \, \mathrm{Im}\{\psi'\})]$$

$$- 2\omega \, \mathrm{Im}\{\mu'\} \, \mathrm{Re}\{(|K_L|^2 \sin^2\theta + K_L' K_S'^* \cos\theta' \cos^*\psi') \, (\sin\theta' \cos^*\psi' - \cos\theta' \sin^*\psi') \, \Phi' A'^*\}$$

APPENDIX B: "SHEARLESS" MEDIA

For a "shearless" material, an arbitrarily large value for shear absorption is chosen, because, as will be shown below, all terms in the expression for power deposition (see Appendix A) which involve reflected (transmitted) shear waves go to zero in the limit that α_S (α_S') goes to infinity. These limits are taken at $x_1 = 0$.

"shear heating" in the unprimed medium ($x_2 > 0$) $= \left(\frac{\omega}{2}\right) |K_S|^2 \, \mathrm{Im}\{\mu\} \, |A|^2 \cosh(4 \, \mathrm{Im}\{\psi\})$

$- 2\omega \, \mathrm{Im}\{\mu\} \, [\mathrm{Re}\{K_L K_S^* (\cos\theta \cos^*\psi - \sin\theta \sin^*\psi) \, (\cos\theta \sin^*\psi + \sin\theta \cos^*\psi) \, \Phi_I A^*\} + \mathrm{Re}\{K_L K_S^* (\cos\theta \cos^*\psi + \sin\theta \sin^*\psi) \, (\cos\theta \sin^*\psi - \sin\theta \cos^*\psi) \, \Phi_R A^*\}]$

"shear heating" in the primed medium ($x_2 < 0$) $= \left(\frac{\omega}{2}\right) |K_S'|^2 \, \mathrm{Im}\{\mu'\} \, |A'|^2 \cosh(4 \, \mathrm{Im}\{\psi'\})$

$- 2\omega \, \mathrm{Im}\{\mu'\} \, \mathrm{Re}\{(|K_L|^2 \sin^2\theta + K_L' K_S'^* \cos\theta' \cos^*\psi') \, (\sin\theta' \cos^*\psi' - \cos\theta' \sin^*\psi') \, \Phi' A'^*\}$

Each term in the above expressions is examined individually below to determine the limit.

$$\text{limit}_{\alpha_S \to \infty} \sin\psi = \left(\frac{K_L}{K_S}\right) \sin\theta = \left(\frac{\omega/c_L - j\alpha_L}{\omega/c_S - j\alpha_S}\right) \sin\theta = 0$$

$$\text{limit}_{\alpha_S \to \infty} \cos\psi = \sqrt{1 - \sin^2\psi} = \sqrt{1 - (0)^2} = 1$$

$$\text{limit } \alpha_s' \to \infty \sin\psi' = \left(\frac{K_L'}{K_S'}\right)\sin\theta = \left(\frac{\omega/c_L' - j\alpha_L'}{\omega/c_S' - j\alpha_S'}\right)\sin\theta = 0$$

$$\text{limit } \alpha_s' \to \infty \cos\psi' = \sqrt{1 - \sin^2\psi'} = \sqrt{1 - (0)^2} = 1$$

$$\text{limit } \alpha_s \to \infty \psi = \text{limit } \alpha_s' \to \infty \psi' = 0$$

$$\text{limit } \alpha_s \to \infty \text{Im}\{\mu\} = \frac{2\rho\omega^3 c_S^3 \alpha_S}{(\omega^2 + c_S^2\alpha_S^2)^2} = 0$$

$$\text{limit } \alpha_s' \to \infty \text{Im}\{\mu'\} = \frac{2\rho'\omega^3 c_S'^3 \alpha_S'}{(\omega^2 + c_S'^2\alpha_S'^2)^2} = 0$$

$$\text{limit } \alpha_s \to \infty |K_S|^2 \text{Im}\{\mu\}|A|^2 = \left(\frac{\omega^2}{c_S^2} + \alpha_S^2\right)\frac{2\rho\omega^3 c_S^3 \alpha_S}{(\omega^2 + c_S^2\alpha_S^2)^2}$$

$$|S_T|^2|L_I|^2 \exp[(\alpha_S + j\left(\frac{\omega}{c_S}\right))x_2 \cos\psi + (\alpha_S - j\left(\frac{\omega}{c_S}\right))x_2 \cos^*\psi] = 0$$

$$\text{limit } \alpha_s' \to \infty |K_S'|^2 \text{Im}\{\mu'\}|A'|^2 = \left(\frac{\omega^2}{c_S'^2} + \alpha_S'^2\right)\frac{2\rho'\omega^3 c_S'^3 \alpha_S'}{(\omega^2 + c_S'^2\alpha_S'^2)^2}$$

$$|S_T|^2|L_I|^2 \exp[(\alpha_S' + j\left(\frac{\omega}{c_S'}\right))x_2 \cos\psi' + (\alpha_S' - j\left(\frac{\omega}{c_S'}\right))x_2 \cos^*\psi'] = 0$$

$$\text{limit } \alpha_s \to \infty K_S^*\Phi_I A^* = \left(\frac{\omega}{c_S} + j\alpha_S\right) S_R^*|L_I|^2 \exp[(\left(\alpha_S + j\left(\frac{\omega}{c_S}\right)\right)\cos^*\psi$$

$$- \left(\alpha_L + j\left(\frac{\omega}{c_L}\right)\right)\cos\theta)x_2] = 0$$

$$\text{limit } \alpha_s \to \infty K_S^*\Phi_R A^* = \left(\frac{\omega}{c_S} + j\alpha_S\right) L_R S_R^*|L_I|^2 \exp[(\left(\alpha_S + j\left(\frac{\omega}{c_S}\right)\right)\cos^*\psi$$

$$+ \left(\alpha_L + j\left(\frac{\omega}{c_L}\right)\right)\cos\theta)x_2] = 0$$

$$\text{limit } \alpha_s' \to \infty K_S'^*\Phi' A'^* = \left(\frac{\omega}{c_S'} + j\alpha_S'\right) L_T S_T^*|L_I|^2 \exp[(\left(-\alpha_S' + j\left(\frac{\omega}{c_S'}\right)\right)$$

$$\cos^*\psi' - \left(\alpha_L' + j\left(\frac{\omega}{c_L'}\right)\right)\cos\theta')x_2] = 0$$

The coefficients of the potentials (Φ_I, Φ_R, A, Φ', A') also depend on the shear absorption coefficient. If the limits as α_S (α_S') goes to infinity of each component of the matrix in Eq. (11) and of each component of the vector on the right-hand side of Eq. (11) are taken before solving the system of equations, the values of S_R and L_R (S_T and L_T) will be finite, not infinite, so the "shear heating" terms are zero as indicated above.

REFERENCES

1. Patzold J, Born H: Behandlung Biologische Gewebe mit Gebundetten Ultraschall. Strahlentherape 76:486, 1945
2. Bell E: The Action of Ultrasound on the Mouse Liver. J Cell Comp Physiol 50:83, 1957
3. Taylor KJW, Connolly CC: Differing Hepatic Lesions Caused by the Same Dose of Ultrasound J Path 98:291, 1969
4. Curtis JC: Action of Intense Ultrasound on the Intact Mouse Liver. *In:* Kelly E (ed.): Ultrasonic Energy, Urbana, University of Illinois Press, 1965, p 85
5. Linke CA, Carstensen EL, Frizzell LA, et al.: Localized Tissue Destruction by High Intensity Focused Ultrasound. Arch Surg 107:887, 1973
6. Carstensen EL: The Mechanism of the Absorption of Ultrasound in Biological Materials. IRE Tran Med Elect ME-7:158, 1960
7. O'Brien, Jr., WD, Shore ML, Fred RK, et al.: On the Assessment of Risk to Ultrasound. *In:* de Klerk J (ed): 1972 Ultrasonic Symp Proc (IEEE Cat# 72 CHO 708-8SU) 1972, pp 486-490
8. Sarvazyan AP: Acoustic Properties of Tissues Relevant to Therapeutic Applications. Br J Cancer 45(Suppl. V):52, 1982
9. Hynynen K: Hot Spots Created at Skin-Air Interfaces During Ultrasound Hyperthermia. Int J Hyperthermia 6(6):1005, 1990
10. Chan AK, Sigelmann RA, Guy AW: Calculations of Therapeutic Heat Generated by Ultrasound in Fat-Muscle-Bone Layers. IEEE Trans Biomed Eng BME-21(9):280, 1974

11. Filipczynski L: Absorption of Longitudinal and Shear Waves and Generation of Heat in Soft Tissues. Ultrasound Med Biol 12:223, 1986

12. Frizzell LA, Carstensen EL: Ultrasonic Heating of Tissues. Electrical Engineering Technical Report No. GM 09933-20, University of Rochester, 1975 (same as Ph.D. Thesis "Ultrasonic Heating of Tissues" by L. A. Frizzell).

13. Frizzell LA, Carstensen EL, Dyro JF: Shear Properties of Mammalian Tissues at Low Megahertz Frequencies. J Acoust Soc Am 60(12):1409, 1976

14. Madsen EL, Sathoff HJ, Zagzebski JA: Ultrasonic Shear Wave Properties of Soft Tissues and Tissuelike Materials. J Acoust Soc Am 74(11):1346, 1983

15. Cooper, Jr. HF: Reflection and Transmission of Oblique Plane Waves at a Plane Interface Between Viscoelastic Media. J Acoust Soc Am 60:1064, 1967

16. Ewing WM, Jardetsky WS, Press F: Two Semi-Infinite Media in Contact. *In:* Shrock RR (ed): Elastic Waves in Layered Media. New York, McGraw-Hill, 1957, pp 83-89

17. Chan AK: Thermal Effects Due to the Propagation of Acoustic Waves in Biological Tissues, Ph.D. Thesis. Seattle, University of Washington, 1971

18. Nyborg WL: Sonically Produced Heat in a Fluid with Bulk Viscosity and Shear Viscosity. J Acoust Soc Am 80(10):1133, 1986

19. Dyro JF: Ultrasonic Study of Material Related to Atherosclerotic Plaque--Dynamic Viscoelastic Properties of Cholesteric Esters, Ph.D. Thesis. Philadelphia, University of Pennsylvania, 1972

20. Carslaw HS, Jaeger JC: Conduction of Heat in Solids, 2nd ed. Oxford, Clarendon, 1959, p 75

21. Goss SA, Johnston RL, Dunn F: Comprehensive Compilation of Empirical Ultrasonic Properties of Mammalian Tissues. J Acoust Soc Am 64(8):423, 1978

22. Goss SA, Johnston RA, Dunn F: Comprehensive Compilation of Empirical Ultrasonic Properties of Mammalian Tissues: II. J Acoust Soc Am 68(7):93, 1980

23. Del Grosso VA, Mader CW: Speed of Sound in Pure Water. J Acoust Soc Am 52(11):1442, 1972

24. Beranek L: The Medium. *In:* Beranek L (ed): Acoustic Measurements. New York, John Wiley & Sons, Inc., 1949, p 68

25. Dyro JF, Edmonds PD: Ultrasonic Absorption and Dispersion of Cholesteryl Esters. Mol Cryst Liq Cryst 25:175, 1974

26. Dyro JF, Edmonds PD: Dynamic Viscoelastic Properties of Cholesteric Liquid Crystals. Mol Cryst Liq Cryst 29:263, 1975